PERGAMON

International Journal of Heat and Mass Transfer 44 (2001) 1343–1371

International Journal of HEAT and MASS TRANSFER

www.elsevier.com/locate/ijhmt

Determination of the quench velocity and rewetting temperature of hot surfaces. Part II: an integrated approach of hydrodynamic–thermodynamic micro- and macro-scale models

M. Ben David [a], Y. Zimmels [a,*], Y. Zvirin [b]

[a] Department of Civil Engineering, Technion – Israel Institute of Technology, Haifa 32000, Israel
[b] Department of Mechanical Engineering, Technion – Israel Institute of Technology, Haifa 32000, Israel

Received 10 June 1999; received in revised form 15 May 2000

Abstract

A new integrated approach, comprising hydrodynamic–thermodynamic micro- and macro-scale models, for analysis of rewetting systems is presented. This new approach facilitates concurrent prediction of rewetting temperature, T^*_{rew}, and quench velocity, U^*_{rew}, for a wide range of system properties. To this end, the previously developed, micro-scale hydrodynamic model is combined with a thermodynamic model and the resulting algorithm is used to derive relations between the quench velocity and rewetting temperature. This combined micro-scale thermodynamic–hydrodynamic model is then interfaced with a known macro-scale model. The former predicts a physically feasible relation between rewetting temperature and quench velocity, as dictated by the physical properties and geometry of the phases involved in the micro-scale, three-phase contact zone. This model uses iterative algorithm that seeks the conditions where the contact angle predicted by the hydrodynamic and thermodynamic models match. Results of application of the combined model to several groups of liquids, with diverse thermo-physical properties, are presented. The calculated rewetting temperature is a monotonic increasing function of the quench velocity, for all liquids investigated, and the contact angle decreases with an increase of temperature. Higher rewetting temperatures and smaller contact angles are produced by increasing the intermolecular force as expressed by the parameter ε_ω/kT_c. The versatility of the model and its sensitivity to small increments in the iteration procedure used in the combined model is demonstrated for the unique case of helium. The mean slope (MS) of the rewetting temperature–quench velocity curve for liquids that pertain to the same group is shown to be nearly invariable. This is a new characteristic property of rewetting systems.

The macro-scale model involves operational constraints that are imposed on the system and consequently a macro-scale relation between the rewetting temperature and quench velocity is set. The intersection between the microscopic, physically feasible, and the macroscopically imposed relations of rewetting temperature and quench velocity yields (T^*_{rew}, U^*_{rew}) that is expected to prevail, for the given conditions of the system. This intersection is required for rewetting to exist. Otherwise, no rewetting is possible, as either complete wetting or non-wetting characterizes the behavior of the system. The new integrated approach is free of the need for assumptions regarding the value of either T_{rew} or U_{rew}, as both are obtained as its output. This work, which completes the series on determination of quench velocity and rewetting temperature on hot surfaces, relies completely on thermo-physical properties of the solid–liquid–vapor system and its operating conditions, without the need for additional assumed inputs. In this sense, the rewetting system can be fully described, once its own micro- and macro-scale properties and constraints are known.

1. Introduction

This work presents an integrated approach whereby a new hydrodynamic–thermodynamic micro-scale model is interfaced with a known macro-scale model of rewetting. The derivation of a combined hydrodynamic–thermodynamic micro-scale model is described first and then the integrated approach is introduced. The hydrodynamic–thermodynamic model, which describes rewetting phenomena, is based on the formulation in [1,2].

* Corresponding author.

0017-9310/01/$ - see front matter
PII: S0017-9310(00)00182-4

Nomenclature

a characteristic molecular size (m)
A Hamaker constant (J)
$\overline{A}$ dimensionless Hamaker constant, $A/6\pi\eta_l U_0 L^2\theta_0$ (dimensionless)
C capillary number, $\eta_l U_0/\sigma\theta_0^3$ (dimensionless)
E parameter, $\lambda_l\Delta T/\rho_l H_l L U_0\theta_0^2$ (dimensionless)
$f(r)$ temperature profile at bottom edge of liquid film (dimensionless)
$F(\bar{r})$ temperature profile at bottom edge of liquid film (K)
F parameter, $\gamma\Delta T/\sigma$ (dimensionless)
$h(\xi)$ liquid–vapor interface profile (dimensionless)
H film thickness (m)
H_l heat of evaporation (J/kg)
k Boltzmann constant (J/K)
L horizontal scaling length, a/θ_0^2 (m)
M molecular weight (kg/kmol)
N parameter, $(L\theta_0\alpha\rho_v H_l^2/\lambda_l T_s^{3/2})(M/2\pi R)^{1/2}$ (dimensionless)
p total pressure, at the bulk density, $p[\rho_\infty]$ (Pa)
p^*_{hs} hard-sphere pressure at the local density, $p^*_{hs}[\rho(z)]$ (Pa)
r radial coordinate (dimensionless)
R universal gas constant (J/kg K)
S parameter, $(L/\sigma\rho_v\theta_0)(\lambda_l\Delta T/L\theta_0 H_l)^2$ (dimensionless)
t time (s)
T temperature (K)
T_{exp} experimental temperature data (K)
T_{in} liquid inlet temperature (K)
T_{mfb} minimum film boiling temperature (K)
T_{leid} Leidenfrost temperature (K)
T_{rew} rewetting temperature (K)
T^*_{rew} rewetting temperature – unique value (obtained as conjugate solution of U^*_{rew}) (K)
T_{solid} initial solid temperature (K)
ΔT characteristic temperature difference, $T_w - T_s$ (K)
ΔT^* temperature step size, in iteration process (K)
$u(r)$ contact line velocity in moving coordinate system attached to the quench front (dimensionless)
u^* contact line (quench front) velocity (dimensionless)
U_{rew} rewetting (quench front) velocity (m/s)
U^*_{rew} rewetting (quench front) velocity – unique value (obtained as conjugate solution of T^*_{rew}) (m/s)
U_0 reference quench front velocity, $K\theta_0^m$ (m/s)
$\overline{v}$ mean velocity of the liquid film (m/s)
x horizontal coordinate in stationary system, along the solid wall (dimensionless)
Y function of μ and ε_ω, Eq. (6) (J per molecule)
z vertical coordinate, normal to the solid wall (dimensionless)

Greek symbols
α molecular accommodation factor, and also used as thermal diffusivity
$\overline{\alpha}$ strength of fluid–fluid intermolecular interaction, Eq. (5)
γ slope of linear $\sigma(T)$ correlation (N/m K)
$\overline{\delta}_1$ half width of solid slab (Fig. 21) (m)
$\overline{\delta}_2$ dimension of outer edge of liquid film (Fig. 21) (m)
ε_ω intermolecular interaction potential, appearing as E_w in the figures (J per molecule)
ε_θ convergence criterion for θ (dimensionless)
η dynamic viscosity (kg/m s)
λ thermal conductivity (W/m K)
λ_r^{-1} typical length of intermolecular interactions (m)
μ chemical potential at the bulk density, $\mu[\rho_\infty]$ (J/kg)
μ^*_{hs} hard-sphere chemical potential, at the local density, $\mu^*_{hs}[\rho(z)]$ (J per molecule)
μ^+_{hs} reference value of the hard-sphere chemical potential, Fig. 1 (J per molecule)
θ contact angle (rad)
θ_h hydrodynamic contact angle (rad)
θ_t thermodynamic contact angle (rad)
θ_0 reference contact angle (rad)
Θ temperature (dimensionless)
ρ density (kg/m^3)
σ surface tension (N/m)
ψ quadratic potential, function of μ and p, Eq. (5)
ξ coordinate (in x-direction) in a moving frame of reference attached to the quench front, $\xi = x - u^* t$ (dimensionless)
$\Delta\xi$ grid size (dimensionless)

Subscripts
A wet region behind quench front (Fig. 21)
B dry region ahead of quench front (Fig. 21)
b bulk of the fluid
c critical
g gas (vapor)
hs hard-sphere
l liquid
lv liquid–vapor
rew rewetting
s saturation
sl solid–liquid
sv solid–vapor
v vapor
w wall (solid)

ξ	differentiation with respect to ξ	*Superscripts*	
(0)	at the wall ($z = 0$)	I	interface (at $z = h$)
1	solid	$(\bar{})$	dimensional variable
2	liquid		

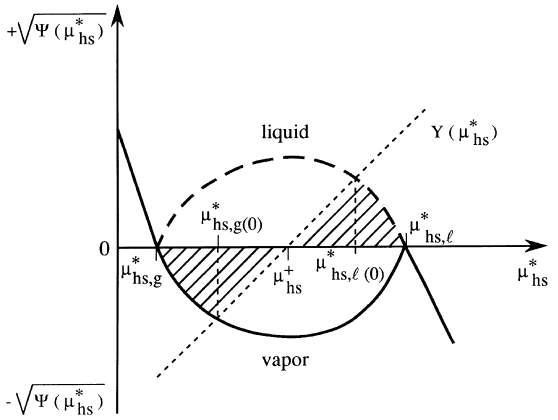

Fig. 1. Graphic description of the parameters given in Eqs. (2)–(6) [10].

The rewetting models have been traditionally classified into two distinct groups, namely thermodynamic and hydrodynamic. It is absolutely clear that using only one of the two approaches does not provide a full physical description of the rewetting problem. Surveys of the rewetting model, including these two approaches have appeared in the literature e.g. [3–7]. Ben David [8], compiled a comprehensive survey of rewetting models, which were partly summarized in [1,2]. Here, the micro-scale hydrodynamic model, as formulated in [1,2], is combined with a thermodynamic model which is based on the work of Sullivan [9,10]. The new approach yields a relation between the quench velocity and the rewetting temperature. The former is set within a predetermined operative range, and each rewetting temperature, which is obtained from the combined model, corresponds to a specific value of this velocity. This gives a micro-scale correlation between the rewetting velocity and temperature. In order to determine the real values of the quench velocity and rewetting temperature for a specific solid–liquid system, the new micro-scale model is interfaced with a macro-scale quench velocity model. The latter accounts for operational constraints, such as flow rate and initial solid temperature. This is done in the second part of this work.

For a specific solid–liquid system, which is set at an initial wall temperature and quench velocity, u^*U_0 (dimensional), the hydrodynamic model produces a solution profile of the liquid–vapor interface equation [2]. This yields an attendant hydrodynamic contact angle. Concurrently, the thermodynamic model, under the same conditions, provides a thermodynamic contact angle. Using an iterative process, the two values of contact angle are compared. In each iteration, the wall temperature is adjusted until a satisfactory convergence between the two models is achieved. Then the wall temperature is recorded, as the rewetting temperature, T_{rew}, at the postulated quench velocity. The calculation is repeated for other values of u^*U_0, and in this way, a rewetting temperature–quench velocity correlation is established for various solid–liquid pairs. In the following, the quench velocity, u^*U_0, is denoted by U_{rew}. The order of magnitude of this velocity is mm/s.

Finally, our new micro-scale model is combined with a macro-scale model, which predicts the quench velocity, U_{rew}, for the given rewetting temperature, T_{rew}, in conjunction with macroscopic operating parameters, e.g., solid properties and liquid flow rate. The result of this integration of models is simultaneous and unique determination of both U_{rew} and T_{rew}.

2. A combined hydrodynamic–thermodynamic micro-scale algorithm

2.1. Theory

2.1.1. The Sullivan model for surface tension and contact angle at the solid–liquid–vapor contact zone

Sullivan [9,10] developed a statistical–mechanical model for the contact angle between a liquid film and a solid substrate. This contact angle, which is considered in the context of the van der Waals model, was previously used by Sullivan to treat gas adsorption on solid surfaces. The model accounts for the occurrence of three types of wetting behavior: complete wetting ($\theta = 0°$), partial wetting ($0° < \theta < 180°$), and non-wetting ($\theta = 180°$), as well as transitions between them. The calculation of intermolecular forces relied on the van der Waals concept of dividing the interaction potential, between a pair of molecules, into a hard-sphere repulsive part and an attractive long-range part. The interaction between the solid substrate and fluid molecules is similarly modeled by a hard-wall repulsive potential, augmented with a long-range attractive part.

Sullivan considered a system in which coexisting liquid and vapor exhibit a contact angle, θ, on the surface of a solid. This contact angle depends on the interfacial tensions at the three-phase contact line by the Young–Dupre equation

$$\cos\theta = \frac{\sigma_{sv} - \sigma_{sl}}{\sigma_{lv}}, \tag{1}$$

where σ denotes interfacial tension and sv, sl, and lv denote the solid–vapor, solid–liquid, and liquid–vapor interface. Using the principles of the mean field theory, he obtained the following expressions for the three interfacial tensions in terms of the chemical potentials:

$$\sigma_{lv} = \frac{1}{\overline{\alpha}\lambda_r}\int_{\mu^*_{hs,g}}^{\mu^*_{hs,l}} \sqrt{\psi\left(\mu^*_{hs}\right)}\,\mathrm{d}\mu^*_{hs,g}, \tag{2}$$

$$\sigma_{sv} = \frac{1}{\overline{\alpha}\lambda_r}\left\{ -\varepsilon_\omega^2 + \int_{\mu^+_{hs}}^{\mu^*_{hs,g(0)}} Y\left(\mu^*_{hs,g}\right)\mathrm{d}\mu^*_{hs,g} - \int_{\mu^*_{hs,g(0)}}^{\mu^*_{hs,g}} \sqrt{\psi\left(\mu^*_{hs,g}\right)}\,\mathrm{d}\mu^*_{hs,g}\right\}, \tag{3}$$

$$\sigma_{sl} = \frac{1}{\overline{\alpha}\lambda_r}\left\{ -\varepsilon_\omega^2 + \int_{\mu^+_{hs}}^{\mu^*_{hs,l(0)}} Y\left(\mu^*_{hs,l}\right)\mathrm{d}\mu^*_{hs,l} + \int_{\mu^*_{hs,l(0)}}^{\mu^*_{hs,l}} \sqrt{\psi\left(\mu^*_{hs,l}\right)}\,\mathrm{d}\mu^*_{hs,l}\right\}, \tag{4}$$

where the subscripts hs, hs,l and hs,g denote hard-sphere, hard-sphere at a liquid phase, and hard-sphere at a gaseous phase. The subscript (0) refers to values of $\mu^*_{hs,g}$ and $\mu^*_{hs,l}$ at the wall ($z = 0$ in our coordinate system, Fig. A12 in [2]). The parameter $\overline{\alpha}$ stands for the strength of the fluid–fluid interaction, and λ_r^{-1} is a typical length which is taken as being identical for both fluid–fluid and wall–fluid interactions.

The functions $\psi\left(\mu^*_{hs}\right)$ and $Y\left(\mu^*_{hs}\right)$ are given by

$$\psi\left(\mu^*_{hs}\right) = \left(\mu^*_{hs} - \mu\right)^2 - 2\overline{\alpha}\left(p^*_{hs} - p\right), \tag{5}$$

$$Y\left(\mu^*_{hs}\right) = \mu^*_{hs} - \mu - 2\varepsilon_\omega, \tag{6}$$

where p and μ correspond to the pressure and chemical potential of the fluid at the bulk density, ρ_∞, and μ^*_{hs} and p^*_{hs} denote the local hard-sphere chemical potential and pressure, $\mu_{hs}[\rho(z)]$ and $p_{hs}[\rho(z)]$, at distance z from the wall. The parameter ε_ω denotes the strength of the wall–fluid interaction.

Fig. 1 describes the function $\sqrt{\psi(\mu^*_{hs})}$ vs. the local hard-sphere chemical potential, μ^*_{hs}. The dashed and solid parts of the curve represent the positive (for liquid) and negative (for vapor) values of $\sqrt{\psi}$, respectively. The parameters $\mu_{hs,g}$ and $\mu_{hs,l}$ in Eqs. (2)–(4) indicate that the state of the fluid at $z \to \infty$, being bulk, is either saturated vapor or saturated liquid, respectively. They are also the roots of the function $\sqrt{\psi(\mu^*_{hs})}$, see Eq. (5) and Fig. 1.

The values of $\mu^*_{hs,g(0)}$ and $\mu^*_{hs,l(0)}$, $\mu^*_{hs,l}$, are obtained at the intersection of the linear function (dotted line) of Eq. (6) with the function $\sqrt{\psi}$ of Eq. (5). The function $Y(\mu^*_{hs})$ intersects the μ^*_{hs} axis at the point μ^+_{hs}. If the intersection point is at $\mu^+_{hs} > \mu^*_{hs,l}$, then a situation of complete wetting ($\theta = 0°$) prevails. If $\mu^+_{hs} < \mu^*_{h,g}$, then a non-wetting situation ($\theta = 180°$) exists. The range $\mu^*_{hs,g} \leqslant \mu^+_{hs} \leqslant \mu^*_{hs,l}$ refers to partial wetting, where the contact angle is between 0° and 180°.

Sullivan [10] notes that the expressions for the solid–fluid interfacial tension (Eqs. 3 and 4) are valid for any thermodynamic state, and they do not necessarily require coexistence of liquid and vapor. When a fluid is in a two-phase state, the solid may interface either with the saturated vapor ($\mu^*_{hs} = \mu^*_{hs,g}$) or with the conjugate liquid ($\mu^*_{hs} = \mu^*_{hs,l}$).

The sum taken over the two integration ranges in expressions (2) and (4) is the magnitude of the common area that is bounded by the curves $\sqrt{\psi(\mu^*_{hs})}$, $Y(\mu^*_{hs})$, and the μ^*_{hs} axis, for values of the arguments between μ^*_{hs} and

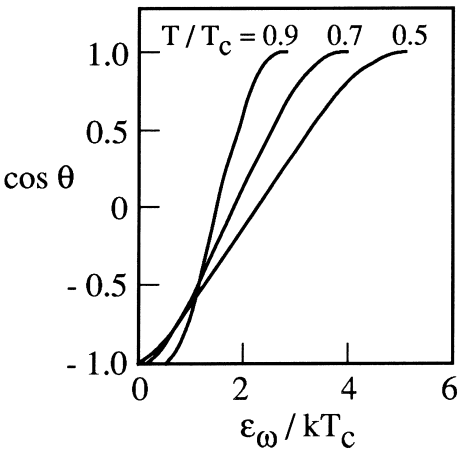

Fig. 2. Behavior of $\cos\theta$ as a function of the parameter ε_ω/kT_c, at three different levels of the reduced temperature, T/T_c [10].

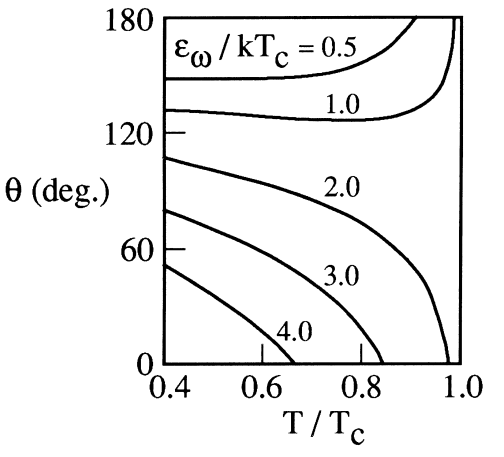

Fig. 3. A plot of contact angle vs. reduced temperature for different values of ε_ω/kT_c [10].

μ^{+}_{hs}. The dashed area on the left-hand side of Fig. 1, between $\mu^{*}_{hs,g}$ and μ^{+}_{hs}, contributes to σ_{sv}, while the area on the right, between μ^{+}_{hs} and $\mu^{*}_{hs,l}$, contributes to σ_{sl}. The difference in magnitudes of these areas, divided by the total area enclosed by $\sqrt{\psi(\mu^{*}_{hs})}$ between $\mu^{*}_{hs,g}$ and $\mu^{*}_{hs,l}$, equals $\cos\theta$ (see Eqs. (1) and (2)). It is clear that the magnitude of the difference in areas in the two cases, $\mu^{*}_{hs} = \mu^{*}_{hs,g}$ and $\mu^{*}_{hs} = \mu^{*}_{hs,l}$, is always less than the total area under the curve $\sqrt{\psi(\mu^{*}_{hs})}$ between $\mu^{*}_{hs,g}$ and $\mu^{*}_{hs,l}$. The interfacial tensions must satisfy the following inequality:

$$|(\sigma_{sv} - \sigma_{sl})| < \sigma_{lv}. \tag{7}$$

Consequently, a contact angle between 0° and 180° is obtained (partial wetting). In this way, the contact angle can be related to the strength of the wall–fluid interaction ε_{w}. Numerical results, giving the relation between ε_{w}

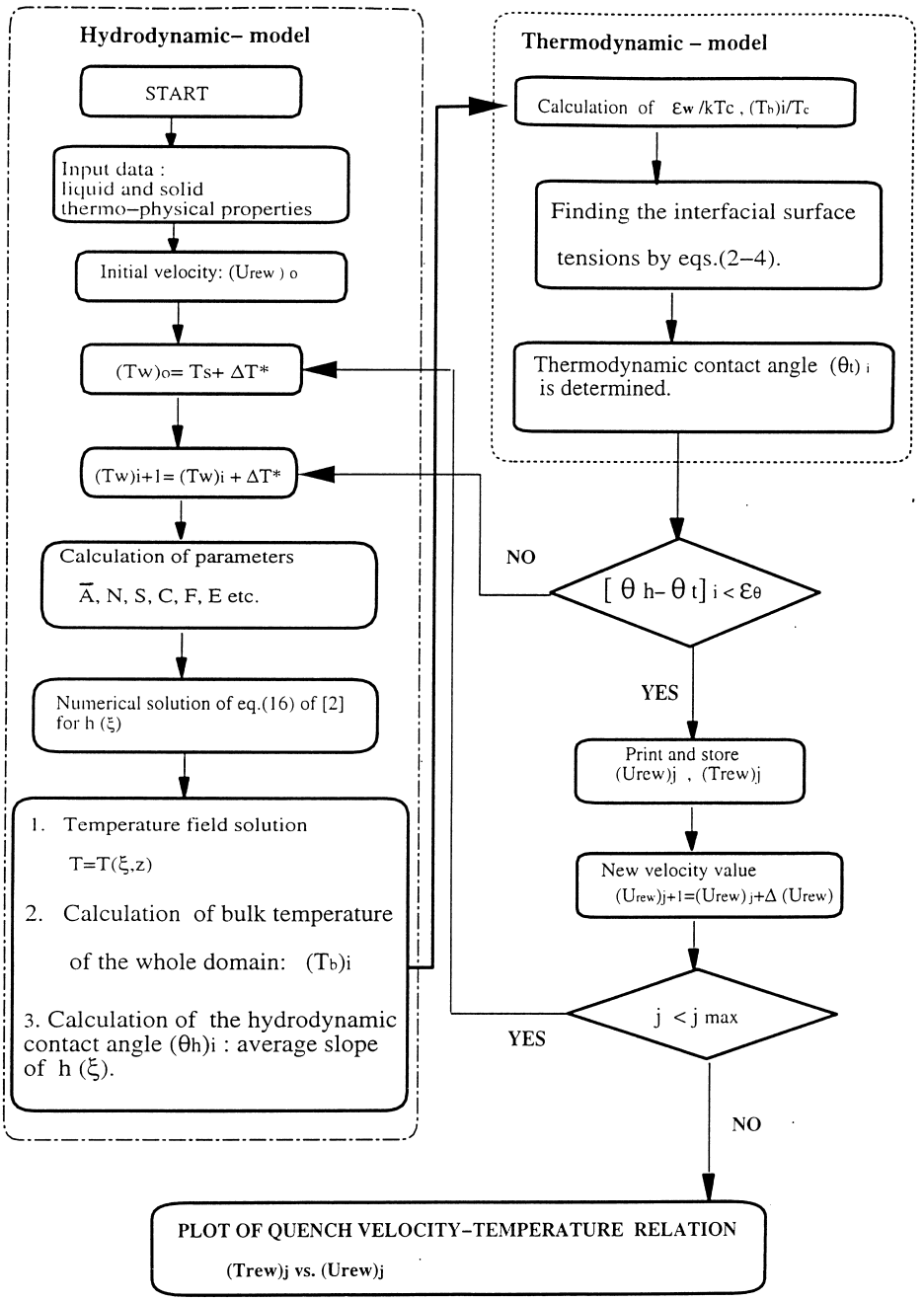

Fig. 4. Structure of the new micro-scale combined thermodynamic–hydrodynamic model algorithm.

Table 1
Thermo-physical properties of fluids at saturation conditions[a]

Properties			Hydrocarbons (organic)		Alcohols (organic)			Polar (inorganic)	
Symbol	Name	Units	Toluene	Benzene	*n*-Butyl	Methanol	Ethanol	Carbon tetrachloride	Water
			C_7H_8	C_6H_6	$C_4H_{10}O$	CH_3OH	C_2H_6O	CCl_4	H_2O
p	Pressure	KPa	103	103	103	103	103	103	103
T_s	Saturation temperature	°C	110.6	80.1	117.7	65	78.4	76.8	100
ρ	Density	kg/m^3	771	815	750	750	737	148	960
ρ_v	Vapor density	kg/m^3	2.96	2.69	2.32	1.19	1.60	3.39	0.600
λ	Thermal conductivity	W/m K	0.136	0.151	0.159	0.190	0.170	0.106	0.680
η	Dynamic viscosity	kg/ms	2.49×10^{-4}	3.16×10^{-4}	3.98×10^{-4}	3.31×10^{-4}	4.33×10^{-4}	4.96×10^{-4}	2.88×10^{-4}
σ	Liquid–vapor interfacial tension	N/m	26.2×10^{-3}	20.1×10^{-3}	16.7×10^{-3}	18.5×10^{-3}	17.8×10^{-3}	20.1×10^{-3}	59.0×10^{-3}
γ	$\gamma = d\sigma/dT$	N/m K	0.015×10^{-3}	0.137×10^{-3}	0.080×10^{-3}	0.094×10^{-3}	0.09×10^{-3}	0.121×10^{-3}	0.18×10^{-3}
T_c	Critical temperature	K	593.8	561.6	560.1	512	516	487.1	647
H_l	Heat of evaporation	J/kg	3.56×10^5	3.95×10^5	5.90×10^5	1.20×10^6	8.41×10^5	1.47×10^5	2.39×10^6
M	Molecular weight	kg/kmol	92.13	78.11	74.12	32.03	46.07	187.3	18
a	Molecular core diameter	nm	0.593	0.527	0.554	0.367	0.445	0.588	0.282
ε/k	Minimum potential of energy divided by Boltzmann constant	K	377	440	351	452	391	327	230.9
T_{rew}	Rewetting temperature	°C $T_{rew} \cong \sqrt{T_s T_c}$	204.3	172	195	143	153	140	218.2

			Gases (inorganic)						Fluorocarbons		
			Carbon dioxide	Sulfur dioxide	Nitrogen	Helium	Ammonia	Bromine	Freon-113	Freon-12	Freon-11
			CO_2	SO_2	N_2	He	NH_3	Br_2	$C_2Cl_3F_3$	CCl_2F_2	CCl_3F
p	Pressure	KPa	718	103	103	103	103	103	103	103	103
T_s	Saturation temperature	°C	−50	−10.02	−195.8	−268.9	−33.2	58.8	47.57	−29.8	23.8
ρ	Density	kg/m^3	1153	1458	808	125	682	3010	1565	1487	1480
ρ_v	Vapor density	kg/m^3	18.0	3.08	1.25	0.178	0.863	7.10	7.38	6.33	5.60
λ	Thermal conductivity	W/m K	0.855×10^{-1}	0.217	0.434×10^{-1}	0.350×10^{-1}	0.540×10^{-1}	0.114	0.380×10^{-1}	0.107	0.864×10^{-1}

η	Dynamic viscosity	kg/ms	1.38×10^{-4}	3.08×10^{-4}	3.00×10^{-4}	0.98×10^{-4}	2.40×10^{-4}	6.90×10^{-4}	5.20×10^{-4}	3.74×10^{-4}	4.20×10^{-4}
σ	Liquid–vapor surface tension	N/m	13.6×10^{-3}	18.5×10^{-3}	8.90×10^{-3}	0.120×10^{-3}	33.6×10^{-3}	38.0×10^{-3}	19.0×10^{-3}	19.0×10^{-3}	18.2×10^{-3}
γ	$\gamma = \mathrm{d}\sigma/\mathrm{d}T$	N/m K	0.177×10^{-3}	0.180×10^{-3}	0.197×10^{-3}	0.093×10^{-3}	0.230×10^{-3}	0.090×10^{-3}	0.100×10^{-3}	0.180×10^{-3}	0.100×10^{-3}
T_c	Critical temperature	K	304	430.2	126	5.25	405.5	583.1	487.1	385	471
H_l	Heat of evaporation	J/kg	3.37×10^{5}	3.90×10^{5}	1.99×10^{5}	2.09×10^{4}	1.37×10^{6}	1.80×10^{5}	1.47×10^{5}	1.67×10^{5}	1.80×10^{5}
M	Molecular weight	kg/kmol	44	64.04	14.006	4.002	17.03	159.8	187.3	120.91	137.7
A	Molecular core diameter	nm	0.449	0.429	0.368	0.257	0.344	0.427	0.492	0.516	0.548
ε/k	Minimum potential energy divided by Boltzmann constant	K	189	252	91.5	10.8	146.8	520	222	286	346
T_{rew}	Rewetting temperature	°C $T_{rew} \cong \sqrt{T_s T_c}$	−12.6	63.2	−174.4	−268.4	39	167	122	33	101

[a] A value of 10^{-20} J is taken for the Hamaker constant.

and θ, which are based on the solution of Eqs. (1)–(4), are shown in Figs. 2 and 3. Note that the data available from Fig. 3, as given by Sullivan [10], are in the $0.5 \leqslant \varepsilon_\omega/kT_c \leqslant 4.0$ range. In this work, the effect of ε_ω/kT_c was tested up to a value of 5.0.

In summary, when the temperature and the interaction energy parameter, ε_ω/kT_c, of a solid–liquid system are known, the contact angle θ can be evaluated by the model of Sullivan [10]. This model was incorporated as part of the new rewetting model developed here because of its useful micro-scale features. These involve intermolecular forces and other physico-chemical aspects that can be related to rewetting phenomena. In order to complete the background, which is necessary for the development of the combined micro-scale model, the thermodynamic and hydrodynamic parts must be interfaced. The details and analysis of the micro-scale hydrodynamic model, as related to contact angle and dynamics of liquid films on a solid surface, are discussed in [1,2].

2.1.2. Computer algorithm for the new thermodynamic–hydrodynamic micro-scale model

Fig. 4 shows a general scheme describing the algorithm which combines the thermodynamic and hydrodynamic parts of the model. In the following, a detailed explanation for this algorithm is presented:

1. Input data of the thermo-physical properties of the liquid and solid are introduced.
2. Initial values of postulated quench velocity, $(U_{rew})_0$, and wall temperature, $(T_w)_0$, which is higher than the saturation temperature, T_s, are set. The index j is used for successive values of the postulated quench velocity $(U_{rew})_j$, and the index i for the wall temperature iteration loop $(T_w)_i$.
3. The dimensionless parameters that appear in the liquid–vapor interface equation [2] are calculated:

$$h_{\xi\xi\xi}\left[1-\frac{F}{1+Nh}\right]+h_{\xi\xi}h_{\xi}\frac{FN}{(1+Nh)^2}+h_{\xi}\left[\frac{2SN^3}{(1+Nh)^3}-\frac{3C\overline{A}}{h^4}+\frac{3NF\theta_0^2}{2h(1+Nh)^2}\right]+\frac{3Cu^*}{h^2}=0. \tag{8}$$

4. A numerical solution of this interface equation is carried out by the IMSL subroutine in order to obtain $h(\xi)$.
5. The hydrodynamic contact angle $(\theta_h)_i$ is calculated from the slope of the line, which is determined by averaging the maxima and minima points of the interface profile, $h(\xi)$.
6. The temperature distribution $\Theta(\xi,z)$, given in [2], is calculated analytically

$$\Theta(\xi,z)=\frac{1+N(h-z)}{1+Nh},\quad 0\leqslant\xi\leqslant 1. \tag{9}$$

7. The liquid bulk temperature, T_b, of the whole flow domain is calculated (see Appendix A).
8. The interfacial surface tensions between the various phases are calculated by the Sullivan model, Eqs. (2)–(4). The results for the thermodynamic contact angle θ_t, that are based on Eq. (1) are shown in Figs. 2 and 3. Using the relevant solid–liquid intermolecular force parameter, ε_ω/kT_c, and the reduced temperature $(T_b)_i/T_c$, the thermodynamic contact angle, $(\theta_t)_i$ is obtained.
9. A comparison between the calculated values of the hydrodynamic, $(\theta_h)_i$, and the thermodynamic, $(\theta_t)_i$, contact angles is made. If the convergence criterion is satisfied, i.e., $|\theta_h - \theta_t|_i \leqslant \varepsilon_\theta$, then the rewetting temperature, $(T_{rew})_j$ is determined. If not, the process continues by taking a new wall temperature, $(T_w)_{i+1} = (T_w)_i + \Delta T^*$, and steps 3–9 are repeated until convergence is established.
10. New values of the quench velocity $(U_{rew})_{j+1}$ are progressively taken, and steps 3–9 are performed until the corresponding rewetting temperatures are determined.
11. A relation is derived between the postulated quench velocity and the rewetting temperature, and it is plotted.

2.2. Derived relation between rewetting temperature and quench velocity – results and discussion

The combined thermodynamic–hydrodynamic model was applied to different groups of fluids, and for each fluid, the rewetting temperatures were determined at different values of postulated quench velocity. Table 1 summarizes the thermo-physical properties of liquids for which rewetting temperatures are reported here. These fluids were selected according to the wide range of their thermo-physical properties, for example, fluids having very low saturation temperatures (helium and nitrogen) in contrast to those with higher values of this temperature (water and toluene). The fluids selected may be categorized into main groups such as: organic, inorganic, polar and cryogenic. The thermo-physical properties, that are necessary as input data for the rewetting model, were taken at saturation conditions and at atmospheric pressure. As an exception, the properties used in the case of CO_2 are saturation conditions at 718 kPa. The thermo-physical properties in Table 1 were taken from the handbooks [11,12]. The molecular interaction parameters, such as ε/k and a, were taken from [13], where ε is the minimum of the potential interaction energy of the liquid and a is the core diameter of a liquid molecule. The parameter ε_ω may be evaluated as a function of the parameter ε and the solid–solid intermolecular force parameter, ε_s. ε_ω/k is one of the factors that defines the thermodynamic contact angle, θ_t (see Figs. 1 and 2). The parameter ε_ω is the minimum of the solid–liquid intermolecular potential of interaction; its evaluation is not simple because of the complexity of the phenomena that gives rise to the intermolecular forces.

Sullivan [10] suggested an approximate method for weighing the solid–solid intermolecular force parameter, ε_s, with that of the fluid–fluid interaction, ε. Since data of ε_ω/kT_c are not readily available for rewetting situations, it is treated as a free parameter. In this way, the sensitivity of calculated rewetting temperatures to a change in the value of this parameter can readily be examined. Another advantage gained by parameterization using the dimensionless group ε_ω/kT_c is the general presentation of the results, i.e., one value of ε_ω/kT_c corresponds to several solids in contact with a single selected liquid. Gerweck and Yadigaroglu [7] evaluated this parameter through contact angle data, at room temperature conditions. However, they used extrapolated values as estimates for the rewetting temperatures. They found that for most liquids on metals, the estimated values of this parameter lead to very small contact angles (see Figs. 1 and 2), which are also associated with rewetting situations. In this context, they showed that the relevant range of ε_ω/kT_c is between 4.0 and 5.0.

The results obtained by applying the new combined model, for the liquids listed in Table 1 are presented in Figs. 5–20. Different scales were applied in the plots in order to provide optimal resolution. Various ranges of ε_ω/kT_c appear in the figures (note that the notation E_w in the figures is identical to ε_ω). This reflects the variability of properties of materials, for which the relation between rewetting temperature and quench velocity is established, and availability of literature data to this end. Each figure consists of four parts that demonstrate the sensitivity of the different plots to variation in ε_ω/kT_c, using three values of this parameter between 4 and 5.

These plots are:

(a) contact angle vs. fluid bulk temperature,
(b) contact angle vs. quench velocity,
(c) rewetting (wall) temperature vs. quench velocity,
(d) fluid bulk temperature vs. rewetting (wall) temperature.

The significance and implications of these results are discussed in the following. These detailed results illustrate the versatility of the new model, as a tool for the simulation of a wide range of solid–liquid–vapor rewetting systems.

The liquids in Table 1 are classified into several groups as follows:

1. *Liquefied refrigerants* (*fluorocarbons*). Freon-11 (R-11), Freon-12 (R-12), Freon-113 (R-113) (Figs. 12–14), carbon tetrachloride, ammonia, sulfur dioxide (Figs. 6, 16, and 19).
2. *Liquefied inorganic gases* (*cryogenic*). Ammonia, helium, nitrogen, sulfur dioxide (Figs. 16–19), bromine (Fig. 15).

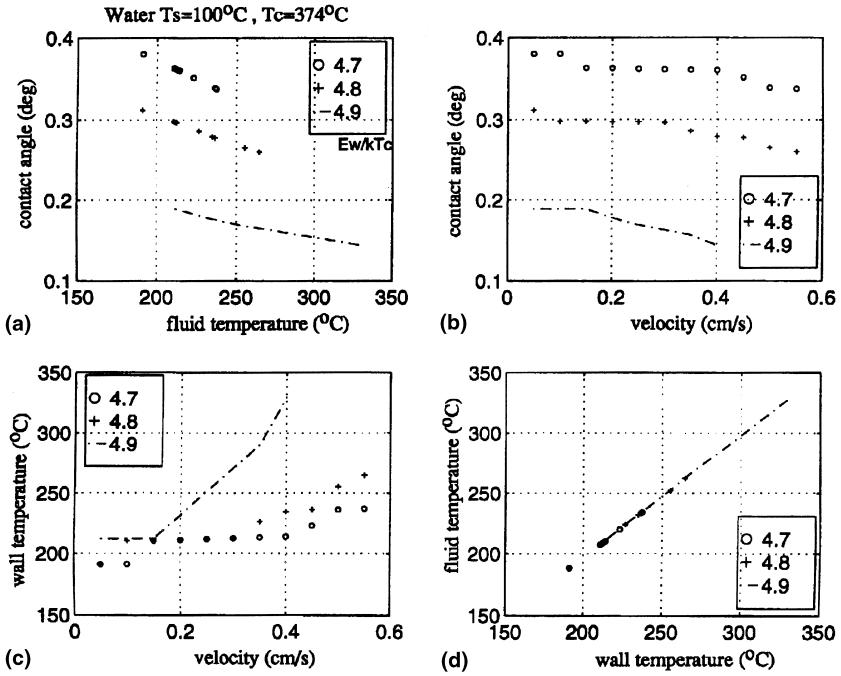

Fig. 5. Results of the micro-scale, thermodynamic–hydrodynamic, model: water on a solid system, for different values of $\varepsilon_{\omega}/kT_c$. $T_s = 100°C$, $T_c = 374°C$: (a) contact angle vs. fluid bulk temperature; (b) contact angle vs. quench velocity; (c) rewetting (wall) temperature vs. quench velocity; (d) fluid bulk temperature vs. rewetting (wall) temperature.

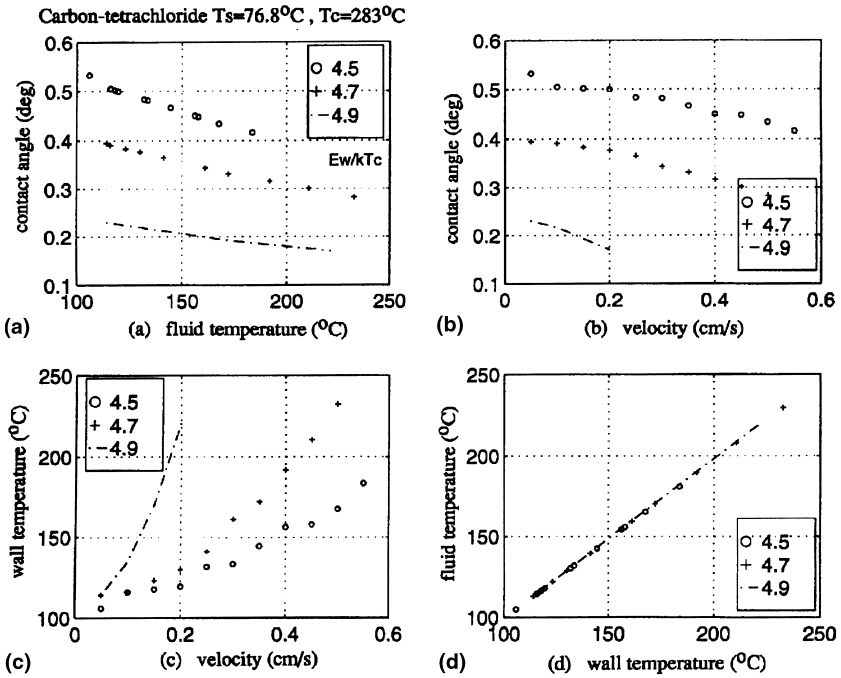

Fig. 6. Results of the micro-scale, thermodynamic–hydrodynamic, model: carbon tetrachloride on a solid system, for different values of $\varepsilon_{\omega}/kT_c$. $T_s = 76.8°C$, $T_c = 283°C$: (a) contact angle vs. fluid bulk temperature; (b) contact angle vs. quench velocity; (c) rewetting (wall) temperature vs. quench velocity; (d) fluid bulk temperature vs. rewetting (wall) temperature.

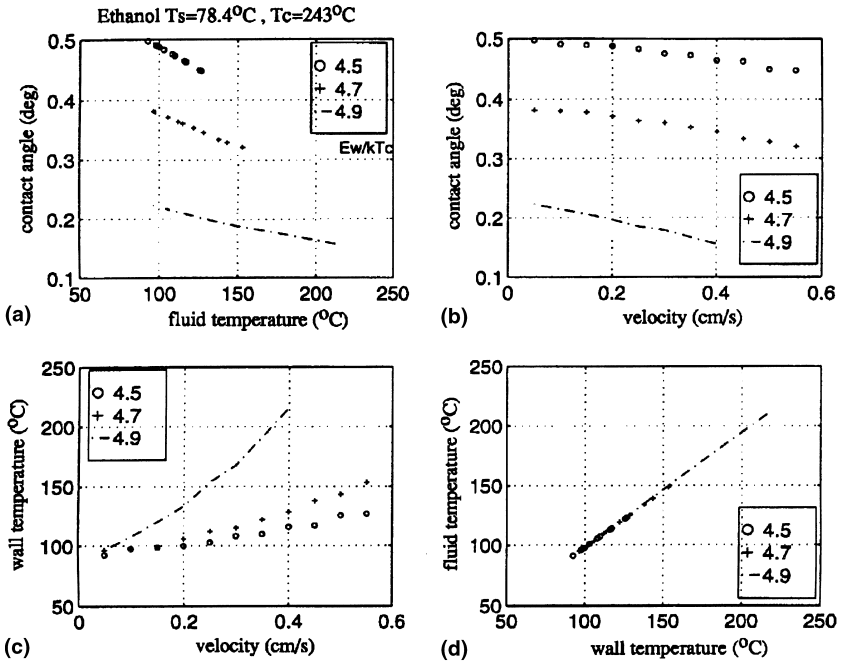

Fig. 7. Results of the micro-scale, thermodynamic–hydrodynamic, model: ethanol on a solid system, for different values of ε_ω/kT_c. $T_s = 78.4°C$, $T_c = 243°C$: (a) contact angle vs. fluid bulk temperature; (b) contact angle vs. quench velocity; (c) rewetting (wall) temperature vs. quench velocity; (d) fluid bulk temperature vs. rewetting (wall) temperature.

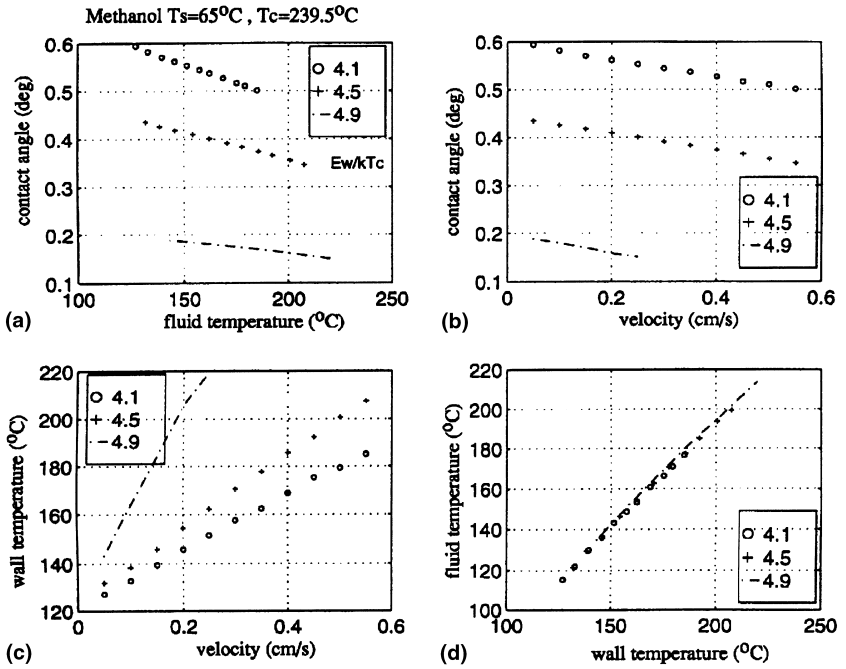

Fig. 8. Results of the micro-scale, thermodynamic–hydrodynamic, model: methanol on a solid system, for different values of ε_ω/kT_c. $T_s = 65°C$, $T_c = 239.5°C$: (a) contact angle vs. fluid bulk temperature; (b) contact angle vs. quench velocity; (c) rewetting (wall) temperature vs. quench velocity; (d) fluid bulk temperature vs. rewetting (wall) temperature.

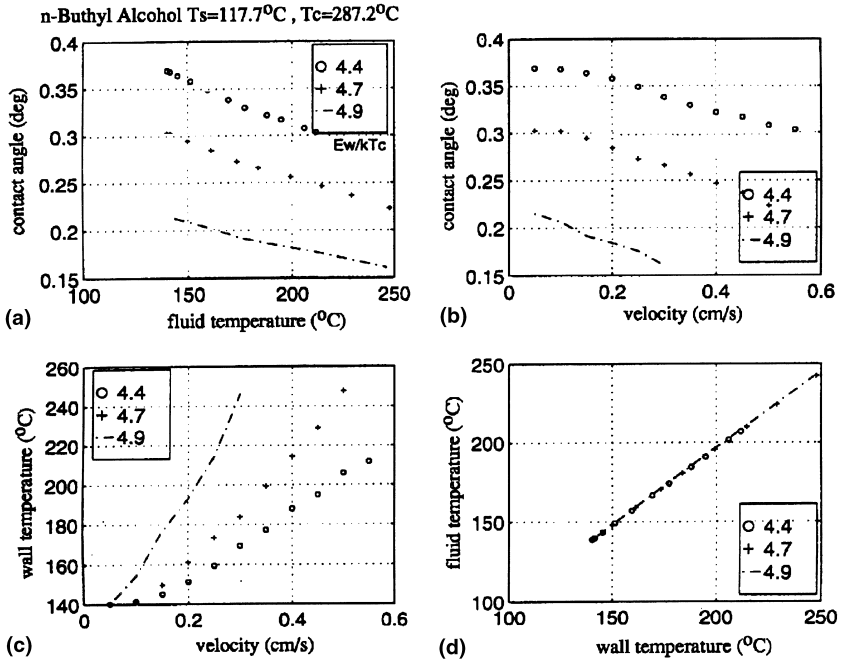

Fig. 9. Results of the micro-scale, thermodynamic–hydrodynamic, model: *n*-butyl alcohol on a solid system, for different values of ε_ω/kT_c. $T_s = 117.7°C$, $T_c = 287.2°C$: (a) contact angle vs. fluid bulk temperature; (b) contact angle vs. quench velocity; (c) rewetting (wall) temperature vs. quench velocity; (d) fluid bulk temperature vs. rewetting (wall) temperature.

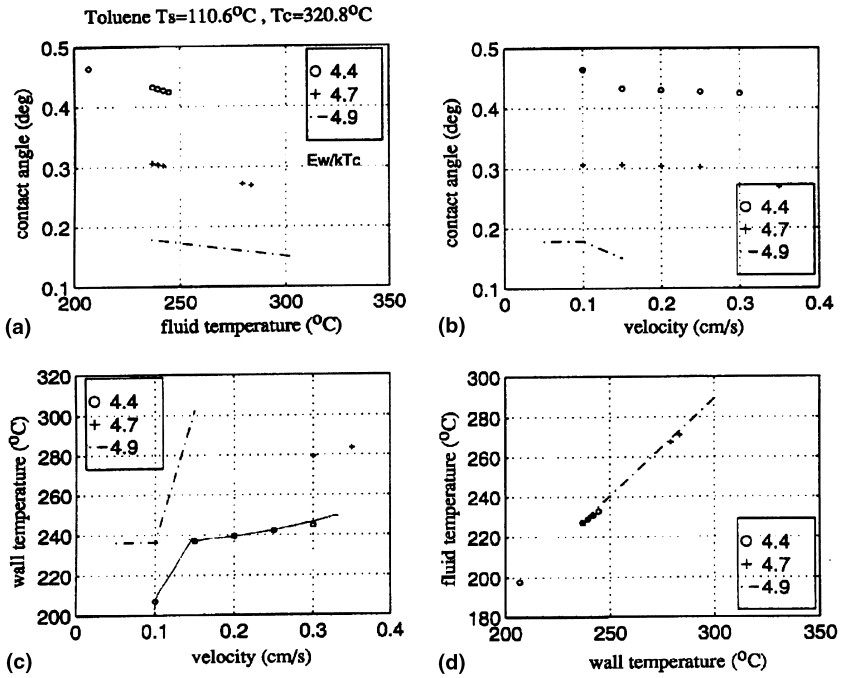

Fig. 10. Results of the micro-scale, thermodynamic–hydrodynamic, model: toluene on a solid system, for different values of ε_ω/kT_c. $T_s = 110.6°C$, $T_c = 320.8°C$: (a) contact angle vs. fluid bulk temperature; (b) contact angle vs. quench velocity; (c) rewetting (wall) temperature vs. quench velocity; (d) fluid bulk temperature vs. rewetting (wall) temperature.

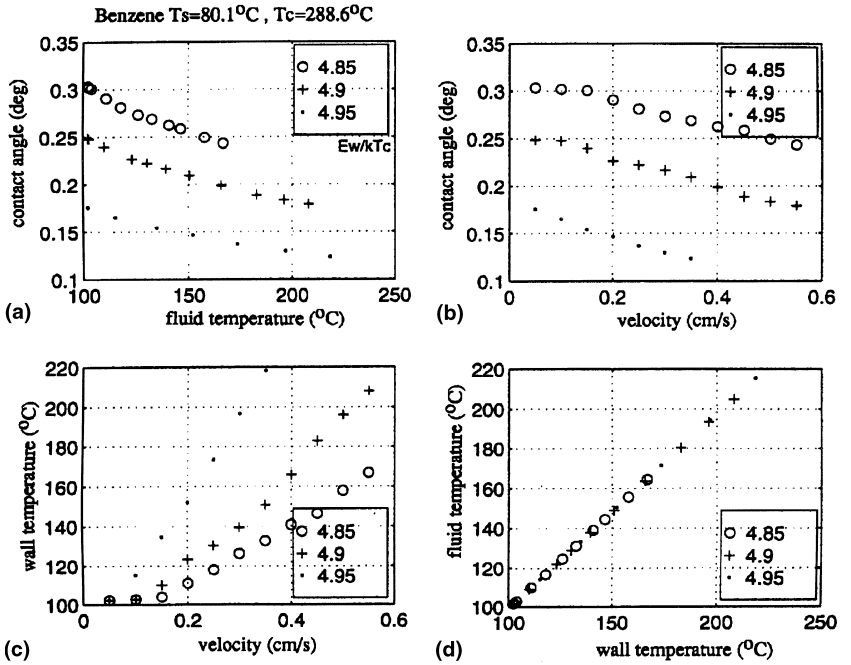

Fig. 11. Results of the micro-scale, thermodynamic–hydrodynamic, model: benzene on a solid system, for different values of ε_ω/kT_c. $T_s = 80.1°C$, $T_c = 288.6°C$: (a) contact angle vs. fluid bulk temperature; (b) contact angle vs. quench velocity; (c) rewetting (wall) temperature vs. quench velocity; (d) fluid bulk temperature vs. rewetting (wall) temperature.

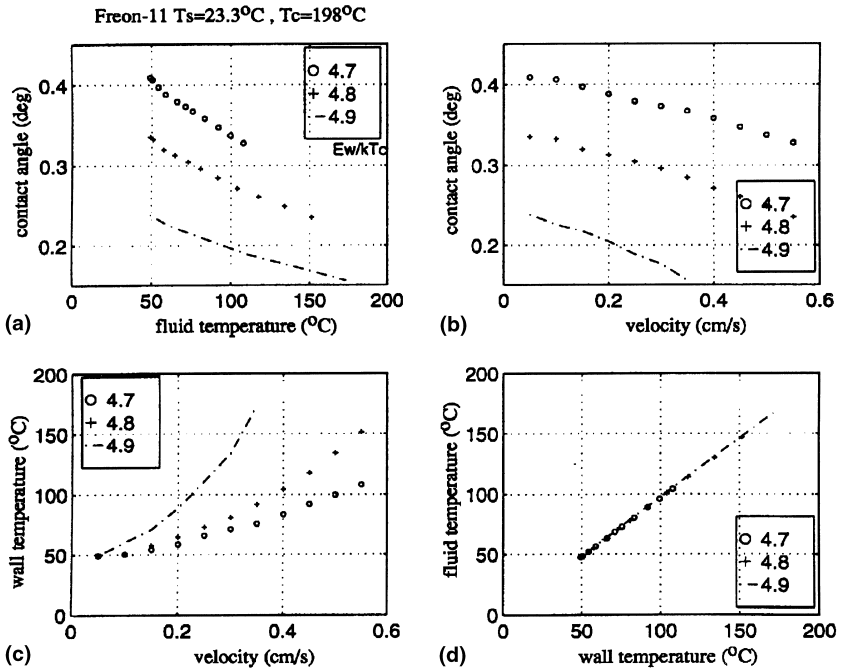

Fig. 12. Results of the micro-scale, thermodynamic–hydrodynamic, model: Freon-11 on a solid system, for different values of ε_ω/kT_c. $T_s = 23.3°C$, $T_c = 198°C$: (a) contact angle vs. fluid bulk temperature; (b) contact angle vs. quench velocity; (c) rewetting (wall) temperature vs. quench velocity; (d) fluid bulk temperature vs. rewetting (wall) temperature.

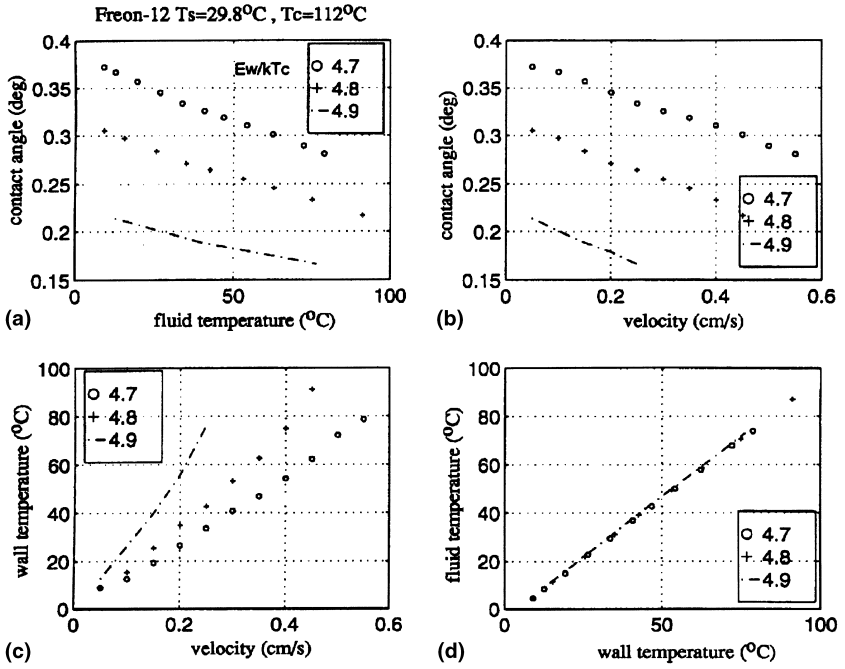

Fig. 13. Results of the micro-scale, thermodynamic–hydrodynamic, model: Freon-12 on a solid system, for different values of ε_ω/kT_c. $T_s = 29.8°C$, $T_c = 112°C$: (a) contact angle vs. fluid bulk temperature; (b) contact angle vs. quench velocity; (c) rewetting (wall) temperature vs. quench velocity; (d) fluid bulk temperature vs. rewetting (wall) temperature.

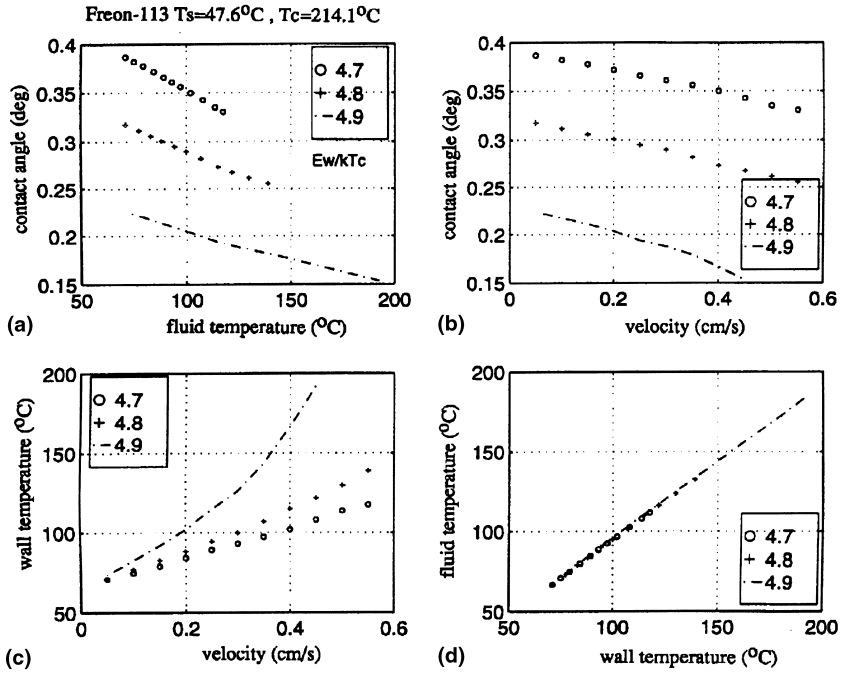

Fig. 14. Results of the micro-scale, thermodynamic–hydrodynamic, model: Freon-113 on a solid system, for different values of ε_ω/kT_c. $T_s = 47.6°C$, $T_c = 214.1°C$: (a) contact angle vs. fluid bulk temperature; (b) contact angle vs. quench velocity; (c) rewetting (wall) temperature vs. quench velocity; (d) fluid bulk temperature vs. rewetting (wall) temperature.

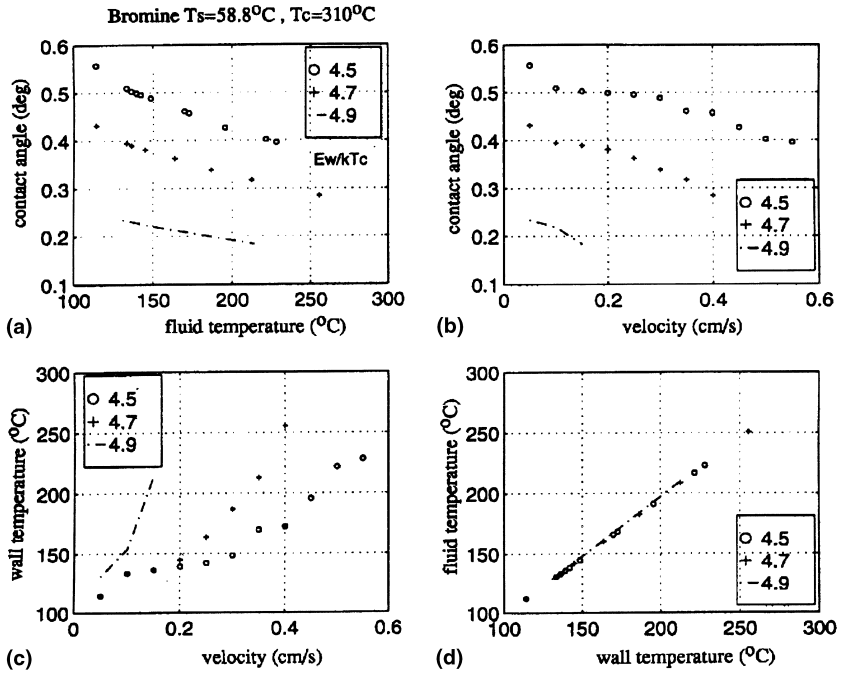

Fig. 15. Results of the micro-scale, thermodynamic–hydrodynamic, model: bromine on a solid system, for different values of $\varepsilon_{\omega}/kT_c$. $T_s = 58.8°C$, $T_c = 310°C$: (a) contact angle vs. fluid bulk temperature; (b) contact angle vs. quench velocity; (c) rewetting (wall) temperature vs. quench velocity; (d) fluid bulk temperature vs. rewetting (wall) temperature.

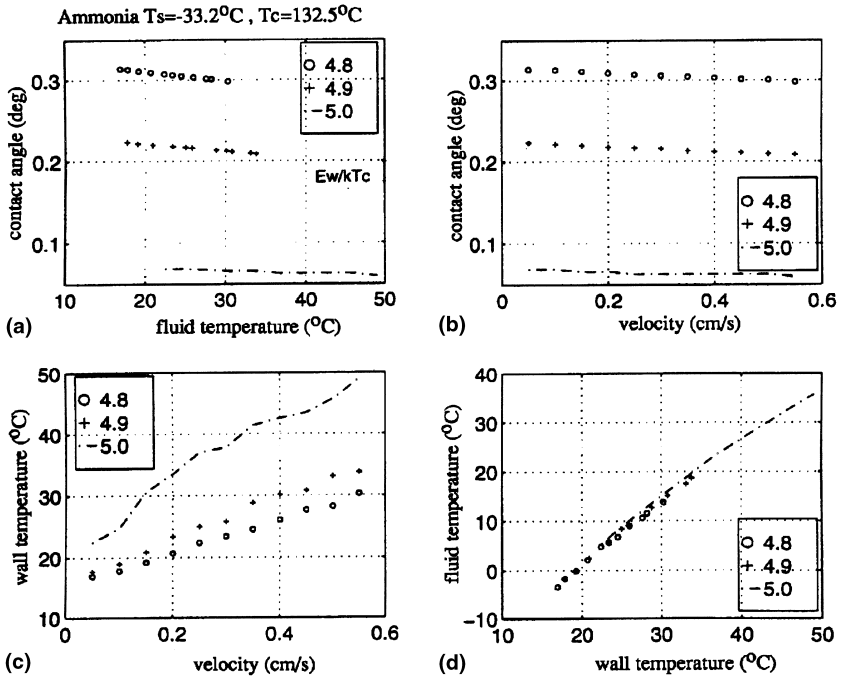

Fig. 16. Results of the micro-scale, thermodynamic–hydrodynamic, model: ammonia on a solid system, for different values of $\varepsilon_{\omega}/kT_c$. $T_s = -33.2°C$, $T_c = 132.5°C$: (a) contact angle vs. fluid bulk temperature; (b) contact angle vs. quench velocity; (c) rewetting (wall) temperature vs. quench velocity; (d) fluid bulk temperature vs. rewetting (wall) temperature.

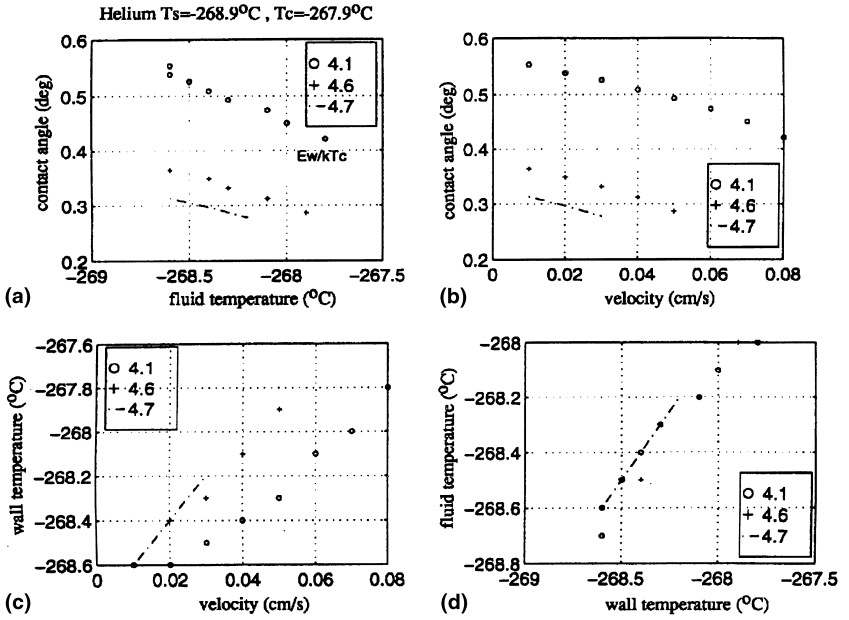

Fig. 17. Results of the micro-scale, thermodynamic–hydrodynamic, model: helium on a solid system, for different values of $\varepsilon_{\omega}/kT_c$. $T_s = -268.9°C$, $T_c = -267.9°C$: (a) contact angle vs. fluid bulk temperature; (b) contact angle vs. quench velocity; (c) rewetting (wall) temperature vs. quench velocity; (d) fluid bulk temperature vs. rewetting (wall) temperature.

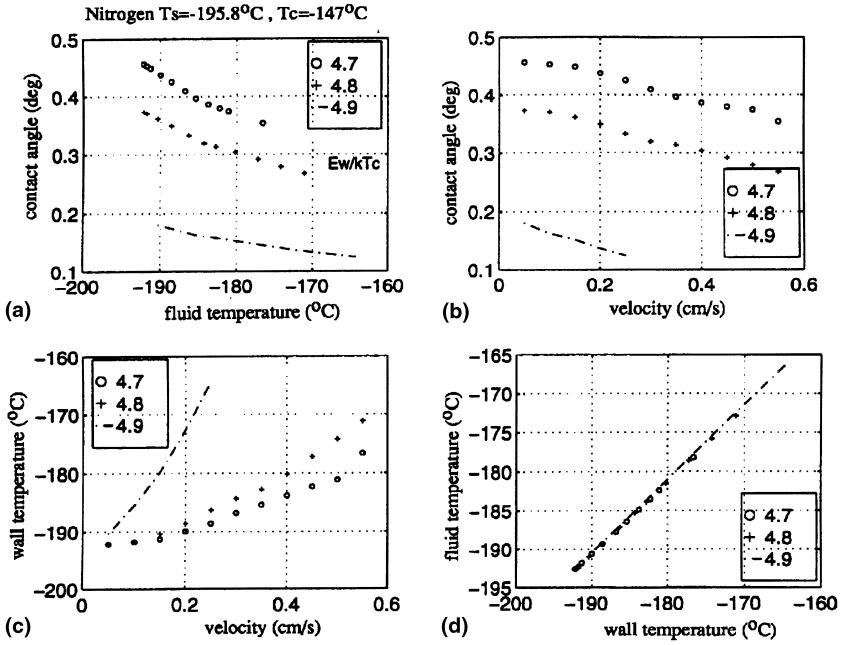

Fig. 18. Results of the micro-scale, thermodynamic–hydrodynamic, model: nitrogen on a solid system, for different values of $\varepsilon_{\omega}/kT_c$. $T_s = -195.8°C$, $T_c = -147°C$: (a) contact angle vs. fluid bulk temperature; (b) contact angle vs. quench velocity; (c) rewetting (wall) temperature vs. quench velocity; (d) fluid bulk temperature vs. rewetting (wall) temperature.

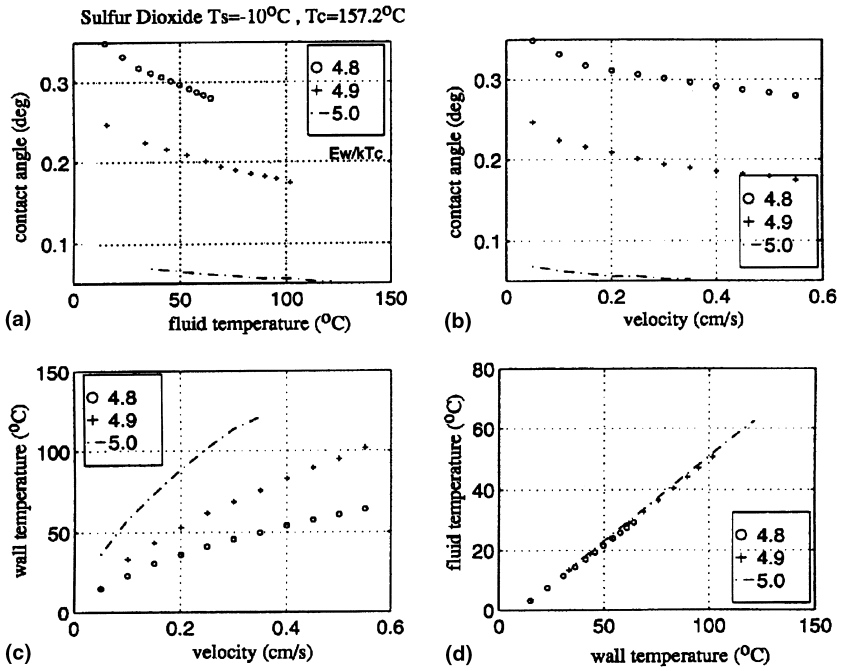

Fig. 19. Results of the micro-scale, thermodynamic–hydrodynamic, model: sulfur dioxide on a solid system, for different values of ε_ω/kT_c. $T_s = -10°C$, $T_c = 157.2°C$: (a) contact angle vs. fluid bulk temperature; (b) contact angle vs. quench velocity; (c) rewetting (wall) temperature vs. quench velocity; (d) fluid bulk temperature vs. rewetting (wall) temperature.

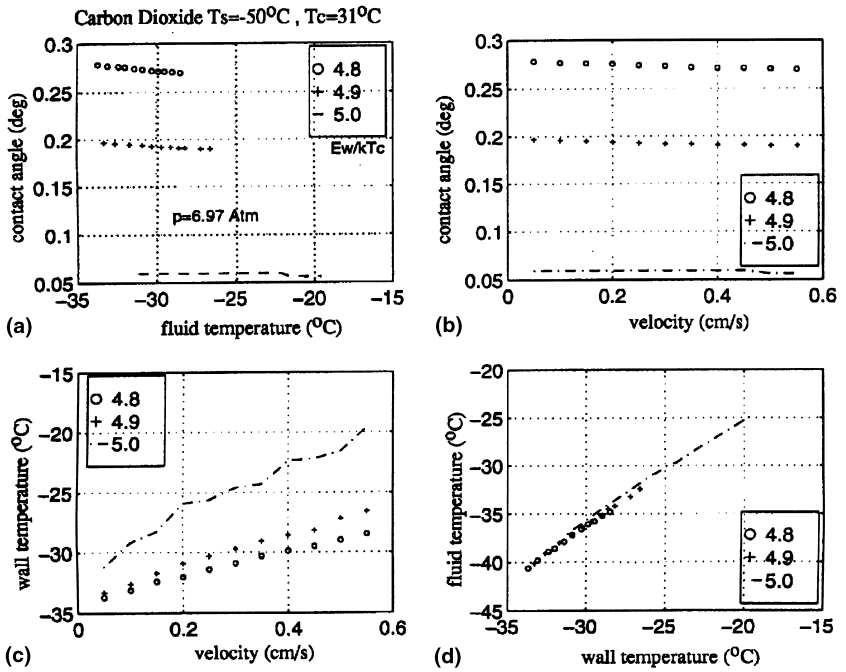

Fig. 20. Results of the micro-scale, thermodynamic–hydrodynamic, model: carbon dioxide on a solid system, for different values of ε_ω/kT_c. $T_s = -50°C$, $T_c = 31°C$: (a) contact angle vs. fluid bulk temperature; (b) contact angle vs. quench velocity; (c) rewetting (wall) temperature vs. quench velocity; (d) fluid bulk temperature vs. rewetting (wall) temperature.

3. *Alcohols* (*organic*). Ethanol, methanol, *n*-butyl alcohol (Figs. 7–9).
4. *Polar* (*inorganic*). Water, carbon tetrachloride (Figs. 5 and 6).
5. *Hydrocarbons* (*organic*). Toluene, benzene (Figs. 10 and 11).

Some of the liquids appear in two different groups and Fig. 20 is for CO_2.

The following common features can be observed for all the solid–liquid systems plotted in Figs. 5–20.

(1) Each point on the curves corresponds to a possible rewetting situation. For instance, fixing a postulated quench velocity (plot (c) in Figs. 5–20), yields a corresponding single value for the rewetting temperature. It follows that the curve actually represents a relation between the postulated quench velocity and its associated rewetting temperature.

(2) In a rewetting situation, the contact angle decreases when the temperature rises (plot (a) in all figures). This physical picture is in agreement with experimental observations that were compiled from several sources by Olek et al. [14] and Carbajo [3]. The contact angles obtained here are smaller than 1° (0.0174 rad). This confirms the validity of the lubrication approximation for rewetting situations, considering the fact that they are characterized by small values of the contact angle ($\theta \to 0$).

(3) The rewetting temperature, T_{rew}, increases with an increase in the quench velocity, U_{rew}, (plot (c) in Figs. 5–20). The plot of T_{rew} vs. U_{rew} is approximately linear in most cases. This relation is one of the important results of this work. In contrast, other prediction models, of either the rewetting temperature or the quench velocity, require that one or both of these parameters be provided as input data. This work provides a direct method, and closed algorithm, for the determination of this temperature–velocity relation. The monotonous increase of the rewetting temperature with the quench velocity may be explained through heat transfer considerations. Higher values of the rewetting temperature at the solid–liquid interface decrease the heat fluxes from the solid (axial conduction for instance) as a result of the smaller temperature gradient at the quench front. The lower gradient follows from the smaller difference between the initial solid temperature (prevailing ahead of and far from the front) and that at the front. Lower heat fluxes produce less intense evaporation and consequently the liquid can advance faster on the solid. This means a higher quench velocity which can be interpreted as a more effective rewetting. Note that this increase in quench velocity was deduced by Olek et al. [4], using their macro-scale model, and through comparison with experimental results of Duffey and Porthouse [15], and others. The quench velocity predicted here is of the order of a few millimeters per second ($U_{\mathrm{rew}} \leqslant 0.6$ cm/s). This range of values was observed experimentally, and also deduced from theoretical quench velocity macro-scale models [4].

(4) All plots of the liquid bulk temperature, T_{b}, as a function of the wall temperature under rewetting conditions, show that the former is lower than the latter. Consequently, heat flows from the wall to the superheated liquid. For liquids with higher conductivity (water, etc.) the difference between these temperatures is smaller. For example, in the case of sulfur dioxide (Fig. 19(d)), this temperature difference is larger than that obtained for water (Fig. 5(d)).

(5) All the results are presented for three levels of $\varepsilon_\omega/kT_{\mathrm{c}}$. Higher values of $\varepsilon_\omega/kT_{\mathrm{c}}$ are characteristic of solids with a stronger attraction to liquid molecules. Therefore, higher levels of $\varepsilon_\omega/kT_{\mathrm{c}}$ are expected to drive the rewetting temperature up (plot (c) in Figs. 5–20), because the liquid tendency to evaporate is reduced. In this context, small changes in $\varepsilon_\omega/kT_{\mathrm{c}}$ can produce, in some liquids, significant changes in the rewetting temperature. In the case of water (Fig. 5(c)) at $U_{\mathrm{rew}} \cong 0.4$ cm/s, the rewetting temperature changes from 240°C, at $\varepsilon_\omega/kT_{\mathrm{c}} = 4.8$, to 320°C at $\varepsilon_\omega/kT_{\mathrm{c}} = 4.9$.

(6) Higher values of $\varepsilon_\omega/kT_{\mathrm{c}}$ (at fixed fluid temperature) induce smaller contact angles (see plot (a) in Figs. 5–20). A stronger attraction of the liquid molecules by the solid (e.g., increase of $\varepsilon_\omega/kT_{\mathrm{c}}$) leads to flatter films with smaller slopes.

(7) Plot (c) in Figs. 5–20 show a general pattern, where the fluid temperature increases with velocity. At low velocity, the rate of increase of temperature with the velocity is small, and in some cases, it practically vanishes. As the velocity increases, the rise in temperature occurs at a faster rate, and in some cases, rather abruptly. This observation can be linked to the behavior of the contact angle (see plot (b) in Figs. 5–20). At low velocity, the contact angle is relatively large, which corresponds to thicker films. The intermolecular attraction forces, being a function of A/H^3, are sensitive to the film thickness H. Consequently, there is a strong effect of the change in velocity, via the film thickness, on the temperature. In some cases, this can appear as an abrupt change in the slope of the temperature vs. velocity curve.

(8) Examination of available rewetting temperature models shows that the spread of predicted values of T_{rew} is quite substantial. For water on stainless steel, these are in a wide range between 180°C and 330°C. This situation arises since these models do not account for all the physical effects involved in rewetting, and they are usually based on either hydrodynamic or thermodynamic approaches. By combining the new micro-scale approach with a reliable macro-scale quench velocity model, the rewetting temperature, as well as the quench velocity, can be determined simultaneously. This is done in the sequel. According to the

results of this work that treats the rewetting problem both thermodynamically and hydrodynamically, the values of the rewetting temperature for water, as an example, are also between 200°C and 330°C (Fig. 5, $\varepsilon_\omega/kT_c = 4.7,\ 4.8,\ 4.9$). However, in this work the temperature range is a consequence of setting up the range of the quench velocity, and not due to a scatter around a specific value of this velocity. For a real problem, which dictates the input data, U_{rew} and T_{rew} are determined together as an output of the combined hydrodynamic–thermodynamic micro- and macro-scale models. This provides a more plausible representation of the actual physical processes involved in the rewetting phenomena.

(9) The quench velocity postulated here, for all the cases studied, is between 0.05 and 0.6 cm/s. This range is based on the results obtained by Olek et al. [4] including comparisons they made with available experimental data. The rewetting temperatures that were obtained for this range of velocities (see plot (c) in Figs. 5–20) are found to be in good agreement, in most cases, with the correlation of Olek et al. [14], see also the last entry in Table 1. Note, however, that their correlation (which does not always fit experimental data) is based on a thermodynamic approach, where the quench velocity is ignored, and only a single value for the rewetting temperature is derived. This value is within the range predicted by our new approach. Plot (c) in Figs. 5–20, shows that the results of the correlation of Olek et al. [14] are good for $0.1 \leqslant U_{rew} \leqslant 0.4$ cm/s and $\varepsilon_\omega/kT_c = 4.9$. If ε_ω/kT_c is larger than or equal to 4.9, then the corresponding quench velocity is of the order of 0.15 cm/s, which is also in the range of the available experimental data. This provides further support for the new quench velocity–rewetting temperature relation that has been derived in this work (see Section 2.3).

The case of helium (Fig. 17) is particularly interesting because of its special thermo-physical properties. The liquid–vapor interfacial tension of helium is very small (0.12×10^{-3} N/m, see Table 1), relative to other common liquids, and its maximum superheat, $T_c - T_s$, is approximately equal to 1°C. The saturation temperature (at 103 kPa) of helium is extremely low (−268.9°C). Nevertheless, the new model provides, once again, very good results as compared with experimental data (see Table 2). In this case, the temperature step size, during the iterative process (Fig. 4), was taken as $\Delta T^* = 0.001$°C (in view of the low superheat of 1°C), and the results obtained during the iterations were sensitive even to this exceptionally small value. The helium case is an excellent example for validation of the model performance. The quench velocities postulated for helium are in the range $0.01 \leqslant U_{rew} \leqslant 0.1$ cm/s. These values are an order of magnitude smaller than those set for other liquids. This may be explained by the lower heat of evaporation of helium, which is approximately 10 times smaller than characteristic values

Table 2
Comparison of results of rewetting temperatures between the new combined model, experimental data, and other models, at atmospheric pressure[a]

Liquid	Range of rewetting temperatures for the postulated quench velocities[b] T_{rew} (°C). Combined new model	Experimental data			Prediction by other models			
		T_{exp}		Solid surface	T_{mfb} or T_{leid}		T_{int} (semi-infinite slab model)	
		(°C)	Ref.		(°C)	Ref.	(°C)	Ref.
Water	200–300	233	[16]	Stainless steel	235	[21]	230	[24]
Carbon tetrachloride	130–200	161.8	[17]	Copper	–	–	158	[17]
Ethanol	149–200	181	[16]	Stainless steel	154.8	[17]	172	[24]
Methanol	125–200	–	–	–	135	[22]	151	[24]
n-Butyl alcohol	140–240	–	–	–	–	–	194	[24]
Toluene	235–300	–	–	–	–	–	221	[24]
Freon-11	50–150	102	[18]	Stainless steel	101.6	[23]	84	[17]
Freon-12	15–80	–	–	–	–	–	48	[24]
Freon-113	70–100	90	[19]	Stainless steel	125.8	[17]	91	[24]
Bromine	125–220	–	–	–	–	–	210	[24]
Benzene	100–220	–	–	–	188.3	–	193.1	[24]
Ammonia	7–35	–	–	–	–	–	67	[24]
Helium	−268.6 to −267.8	−268.7	[17]	–	−268.7	[17]	−268.56	[24]
Nitrogen	−190 to −170	−177	[20]	Copper	−179.2	[17]	−179	[24]
Sulfur dioxide	20–90	–	–	–	–	–	82	[24]
Carbon dioxide (at $p = 6.97$ atm)	−32 to −23	–	–	–	–	–	−24	[24]

[a] The data in this table were compiled from Olek et al. [4] and Gerweck [5].
[b] The postulated quench velocity range is 0.05–0.6 cm/s.

of other fluids that are listed in Table 1. In other words, faster evaporation of the helium at the quench front slows its quench velocity, compared to other less volatile liquids.

2.3. Comparison with other models and experimental data

As noted previously, most of the existing models for the rewetting temperature are based on either thermodynamic or hydrodynamic approaches [1]. The rewetting temperature–quench velocity relation, derived here, is based on consideration and interfacing of both. Therefore, it is interesting to compare this new combined approach with each of the separate approaches. Other types of predictions are usually based on the minimum film boiling, or the Leidenfrost temperature that is obtained from semi-empirical correlations. In Table 2, several fluids, at atmospheric pressure conditions are compared. The data in Table 2 were compiled from [4,5], except for the T_{int} column that was calculated here. The results of T_{rew} in Table 2 are represented by a range of values according to the rewetting temperature–quench velocity relations plotted in Figs. 5–20. The other results are expressed as discrete values, in accordance with the correlation or experimental data used. Evidently, the range of predicted temperatures (second column from left in Table 2) shows a satisfactory agreement with results of the other models. In the following section, discrete values for both the rewetting temperature and quench velocity (for the simulated solid–liquid systems) are obtained. The quench velocity values are of the order of few millimeters per second, as deduced from experimental data collected by Olek et al. [4]. The temperature ranges given in Table 2 were selected, using the assumption that the postulated quench velocity is approximately in the range $0.05 \leqslant U_{rew} \leqslant 0.6$ cm/s (see Figs. 5–20). The satisfactory agreement with experimental data and other models provides an adequate verification of the validity of the new model and its predictions.

For comparison, three fluids of three different categories are discussed. Water (polar), methanol (organic) and helium (inorganic) were selected for this purpose, because of the great variety of their thermo-physical properties. For example, the heat of evaporation of water is highest (2.39×10^6 J/kg, cf. Table 1) among all the liquids studied here, whereas helium has the lowest value (2.09×10^4 J/kg). Methanol, which is organic, lies in the intermediate range (1.20×10^6 J/kg). The saturation temperature, T_s, as well as the critical temperature, T_c, are quite different. The rewetting temperature values predicted for water, methanol and helium are in the ranges 200–300°C, 125–200°C and from −268.6 to −267.8°C. These ranges correspond to the postulated range for quench velocity between 0.05 and 0.6 cm/s (see plot (c) of Figs. 5 and 8), and between 0.01 and 0.08 cm/s (plot (c) of Fig. 17).

For water, the rewetting temperature range spans the highest predicted values, this being in agreement with its largest heat of evaporation. This fact allows the water to be in contact with the hot surface at a higher level of superheating, in contrast to helium, which has a stronger tendency to evaporate. This also explains the low quench velocities obtained for helium (O(10^{-2} cm/s)), which are lower by an order of magnitude than those obtained for water and methanol (O(10^{-1} cm/s), plot (c) of Figs. 5, 8 and 17). Another feature that can be observed is the different relation between the wall and the bulk liquid temperatures, T_w and T_b (plot (d) of Figs. 5, 8 and 17). For water, the difference between them is quite small ($\Delta T = T_w - T_b \cong 2$°C), for methanol $\Delta T \cong 10$°C and for helium $\Delta T \cong 0.1$°C. This behavior follows from the difference of the thermal conductivities of the three liquids. The values of λ for water, methanol and helium are 0.680, 0.190 and 0.035 W/m K, respectively. Thus, for water, with higher λ than methanol, the temperature difference, ΔT, is relatively small. In the case of helium, which has the lowest value of λ, there is a strong effect of superheat, which is very low, causing small ΔT and also a stronger dependence of T_b on T_w (steeper slope in plot (d) of Fig. 17). The maximum superheat, $T_c - T_s$, for water, methanol and helium are 374°C, 174°C and 1°C, respectively (see Table 1). The dimensionless ratio $(T_b - T_s)/(T_c - T_s)$, calculated for the three liquids, is approximately 5.3×10^{-3}, 5.7×10^{-2} and 10^{-1}, respectively. This result clearly explains the two observed phenomena, mentioned above, e.g., of small ΔT, and strong correlation of T_b and T_s for helium, as compared to water and methanol, despite the fact that helium has very low saturation and critical temperatures.

2.4. The mean slope of the temperature–velocity relation

The temperature–velocity relations shown in plot (c) of Figs. 5–20 are monotonous ascending functions. A mean slope (MS) of the curves was evaluated using end values of rewetting temperatures and velocities in the range investigated.

For all the fluids studied, this MS is in the range between 0.001 and 0.070 cm/s K (see Table 3). In several groups of fluids the value of the MS is within a narrow range. For example, all fluids in the fluorocarbon group show MS values of ~0.006, whereas in the case of alcohols and polar groups, half of this value, i.e., ~0.003 applies. This unique behavior of the MS may explain why the expected rewetting temperatures fit very well the experimental data, notwithstanding the great variance of the fluids studied. In other words, it is possible to extend these results, which

Table 3
The mean slope (MS) of the rewetting temperature–quench velocity relation for different fluids[a]

Subgroup: liquid	T_s (K)	T_c (K)	T_s/T_c	ε_ω/kT_c	MS (cm/s K)
Polar					
Water	373	647	0.577	4.9	0.0033
Carbon tetrachloride	350	487	0.719	–	0.0032
Alcohols					
Ethanol	351.4	516	0.681	4.9	0.0035
Methanol	338	512	0.66	4.9	0.0036
n-Butyl	390.7	560	0.698	4.9	0.0029
Hydrocarbons					
Benzene	353	562	0.628	4.9	0.0086
Toluene	383.6	594	0.645	4.9	0.0037
Liquefied gases					
Bromine	332	583	0.569	4.9	0.0014
Nitrogen	77.2	126	0.613	4.9	0.0185
Helium	4.1	5.25	0.78	4.9	0.033
Ammonia	240	406	0.591	4.9	0.032
Sulfur dioxide	263	430	0.612	4.9	0.0058
Carbon dioxide (6.97 atm)	223	304	0.733	4.9	0.071
Fluorocarbons					
Freon-11	296.8	471	0.630	4.8	0.0056
Freon-12	243.2	385	0.631	4.8	0.0055
Freon-113	321	487	0.659	4.8	0.0063

[a] $\varepsilon_\omega/kT_c = 4.8$, 4.9, and atmospheric pressure.

are based on the rewetting temperature–quench velocity relation obtained here, for other different groups of fluids. For example, in spite of the fact that the saturation temperatures of water and helium are very different, and their superheat temperature differences are far apart ($\Delta T \cong 274$°C for water and 1°C for helium), their MS values are in the relatively narrow range mentioned above.

3. Integrated approach of micro- and macro-scale models

3.1. Principle of model integration

Each point of the rewetting temperature–quench velocity relation represents a possible rewetting situation, i.e., for each selected value of the quench velocity, U_{rew}, the combined thermodynamic–hydrodynamic model determines the appropriate rewetting temperature, T_{rew}. Note that T_{rew} and U_{rew} are also functions of the solid thermo-physical properties, and of the initial solid temperature, solid thickness, inlet liquid temperature and mass flow rate. These macroscopic parameters characterize the operating conditions of the solid–liquid flow system studied. For a given solid–liquid system that is operating under specified flow and temperature conditions, the values of T_{rew} and U_{rew} are unique. Thus, the intersection of the new micro-scale model with one of the known macroscopic models for the quench velocity, completes the algorithm that determines T^*_{rew} and U^*_{rew}. To this end, our new micro-scale model is combined with the macroscopic quench velocity model of Olek et al. [4]. The latter was selected in view of its versatility, and its main features, as compared to other models, are briefly presented here.

3.2. Macroscopic models

Prediction of the rewetting velocity has been the primary goal of many investigations of the rewetting problem. Reviews on the subject were published by Swan and Carbon [25], Butterworth and Owen [26], Elias and Yadigaroglu [27,28], Carbajo and Siegel [29], and Ben David [8]. Theoretical models for this problem involve the solution of the Fourier heat conduction equation in the solid for specified boundary conditions, that are representative of the heat transfer processes at the surface of the solid. The one-dimensional models typically assume a uniform temperature distribution in the solid, in the direction perpendicular to the liquid flow.

In most of these models, the heat transfer coefficient is chosen as a constant that is large in the wet region behind the quench front and zero in the dry region ahead of it. With a suitable choice of the heat transfer coefficient and the rewetting temperature, these models can predict the rewetting velocity quite well for low coolant flow rates. However, at high flow rates, extremely high values of the heat transfer coefficient must

be postulated in order to fit results of a specific one-dimensional model with experimental data. In order to overcome this problem, two-dimensional models were developed. For example, Elias and Yadigaroglu [27], and others, derived more advanced two-dimensional models, but they require that the heat transfer coefficient and rewetting temperature must be given as input parameters. It is obvious that by using these two "degrees of freedom", one can obtain reasonable fit with different experimental data. Olek et al. [4] achieved remarkable progress by developing a new model, wherein the only required input parameter is the rewetting temperature. The heat transfer coefficient is obtained as part of their model solution. They considered the rewetting process as a conjugate heat transfer problem, and formulated the energy balance equations both in the solid (conduction) and in the liquid (conduction and convection). A simultaneous solution of the energy equations eliminates the a priori requirement of data of the heat transfer coefficient. This is the main reason for selecting the Olek et al. [4] model as a macro-scale model in this work. A combination of the new micro-scale model, with that of Olek et al. [4], facilitates the determination of the rewetting temperature and quench velocity, as an intersection output of the macro–micro-scale model. A brief presentation of the macro-scale model of Olek et al. [4] is given in Appendix B, as a background to its incorporation in this work.

3.3. Theoretical considerations and solution algorithm

The micro-scale hydrodynamic–thermodynamic model sets a physically feasible relation between the rewetting velocity and temperature, U_{rew} and T_{rew}, i.e., the quench front velocity and the rewetting temperature at the solid–liquid–vapor contact line. In order to determine uniquely the values of U^*_{rew} and T^*_{rew} for a given solid–fluid pair and operating conditions, an additional relation between U_{rew} and T_{rew} is needed. This relation can be obtained from an existing macro-scale model representing the rewetting process. Several models to this end have been suggested (cf. the reviews [8,25–29]). Most of these models rely on several arbitrary input parameters, and consequently, they are not compatible with the method presented here. Therefore, as previously mentioned, we have adopted the method developed by Olek et al. [4], whereby the rewetting velocity is calculated, by solving a conjugate heat transfer problem, using the rewetting temperature as the only arbitrary input. Other parameters, and in particular, the local heat transfer coefficient, are obtained as part of the solution for any solid–liquid pair and operating conditions, e.g., initial solid temperature and liquid flow rate. The values of U^*_{rew} and T^*_{rew} are uniquely determined incorporating both the micro- and macro-scale models and solving the equivalent of two equations for the two unknowns.

The governing equations of the macro-scale model developed by Olek et al. [4] appear in Appendix B. The model is based on posing the heat transfer problem as a conjugate one, and solving simultaneously the energy equations in three domains: conduction in the dry and wet regions of the solid (ahead of and behind the quench front) and convection in the liquid.

For a given solid–liquid system that is operating under pre-determined conditions, the set of conjugate equations of the macroscopic model [4] in Appendix B, is solved for a range of postulated values of the rewetting temperature, T_{rew}. The quench velocity, U_{rew}, is then obtained as the output. The new thermodynamic–hydrodynamic micro-scale model generates independently another relation between U_{rew} and T_{rew}.

The macroscopic relation defines a possible range of rewetting situations that are imposed on the system as macro operating conditions, e.g., inlet velocity and initial solid temperature. The micro-scale rewetting temperature–quench velocity relation provides the information on constraints that are imposed by the solid–liquid–vapor interactions, at the three-phase contact zone. The intersection of these two rewetting temperature–quench velocity relations, determines uniquely the prevailing values of T_{rew} and U_{rew}, e.g. (T^*_{rew}, U^*_{rew}). Thus, the interfacing between the macro and micro models leads to a closed algorithm, where no external arbitrary input data of either T_{rew} or U_{rew} are required.

3.4. Interfacing between the macro- and micro-scale models – a new integrated approach for rewetting systems

The new approach of interfacing between the micro- and macro-scale models was applied to three solid–liquid rewetting systems: water on stainless steel, nitrogen on copper and Freon-113 on stainless steel. These three cases are representative of three different rewetting classes according to their physical and chemical properties. The water is classified as a polar liquid, the nitrogen as inorganic and cryogenic, and Freon-113 (also known as R-113) belongs to the fluorocarbons group. These cases were studied by Olek [30], who compared his model results to experimental data. The fit he established between theory and experiment is best for cases of low flow rates per unit wetted perimeter (up to $\sim$0.05 kg/ms). Therefore, these cases were selected here in order to incorporate the macro model and validate the new approach. Details of the selected systems, which were presented by Olek [30] are summarized in Table 4 (see Fig. 21).

Figs. 22–24 show plots of rewetting temperature vs. quench velocity for the water/stainless steel, nitrogen/copper, and Freon-113/stainless steel systems simulated by the macro and micro rewetting models. Each figure has four plots (a)–(d), for four different initial solid temperatures (for e.g., 400°C, 500°C, 600°C and 700°C,

in the case of water on stainless steel). The plots include five curves, three of which pertain to the macro-scale flow rate per unit wetted perimeter (0.017, 0.047, and 0.11 kg/ms) and the other two to the solid–liquid interaction parameter of the micro-scale model ε_ω/kT_c (4.1 and 4.9). Note that the selected flow rates were used by Olek [30] to compare the results of his model with the experimental data of [15]. The three flow rate levels cover the operational range of the systems treated by Olek [30], and the solid–liquid interaction parameter ε_ω/kT_c covers a range which is typical of solid–liquid systems that are simulated by the micro-scale model.

In order to illustrate the effect of the solid–liquid intermolecular forces on T_{rew} and U_{rew}, the parameter ε_ω/kT_c was varied in the range $4 \leqslant \varepsilon_\omega/kT_c \leqslant 5$. Both the relations for rewetting temperature vs. quench velocity, obtained by the micro- and macro-scale models, are monotonous, but they differ in their slopes. Consequently, there are "micro-scale" curves that intersect the three "macro-scale" curves, each at a different point. These intersection points provide predictions of the quench velocity and the rewetting temperature that are based on the physical properties of specific solid–liquid systems and their operating conditions. This means that the values of both T^*_{rew} and U^*_{rew} are determined theoretically as a unique intersection point, as determined by the two approaches and the two micro- and macro-scale models. The interfacing between the two models results in the new integrated approach for the simulation of rewetting phenomena.

3.5. Analysis of results and discussion

The intersection of the "micro" and "macro" monotonous relations, such as in Figs. 22–24, deter-

Table 4
Details of three solid–liquid macro systems studied by Olek [30]

Solid–liquid system	Thickness of solid rod (mm)	Diameter of solid rod (cm)	Inlet liquid temperature (°C)	Initial solid temperatures (°C)
Water/stainless steel	0.50	0.627	20.0	400, 500, 600, 700
Nitrogen/copper	1.08	2.223	−171.0	−100, −60, −40, −10
Freon-113/stainless steel	2.00	1.600	29.6	120, 160, 180, 200

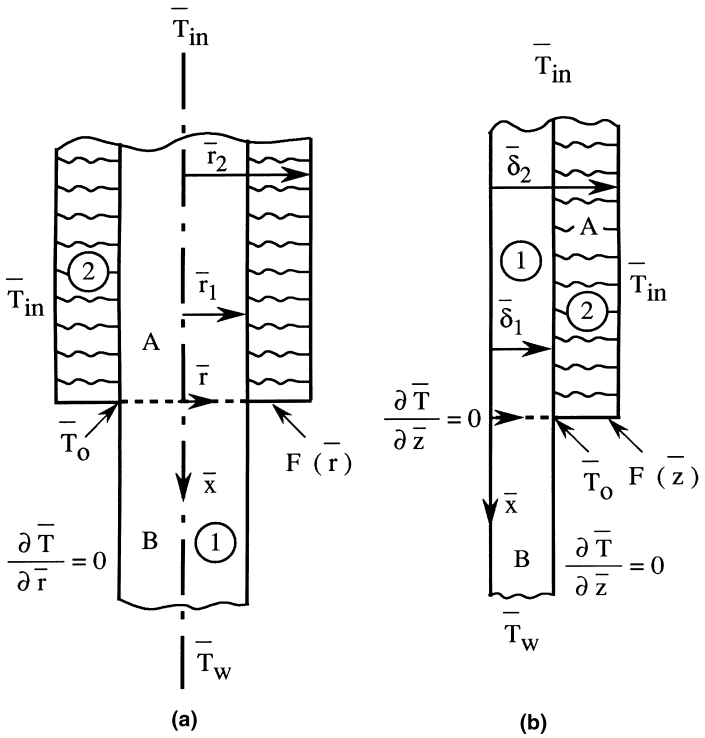

Fig. 21. Scheme of problem geometry, rewetting of hot surfaces in top flooding: (a) cylindrical geometry; (b) cartesian geometry. $F(\bar{r})$ or $F(\bar{z})$ are general functions of the assumed boundary conditions for the temperature at the quench front line [4].

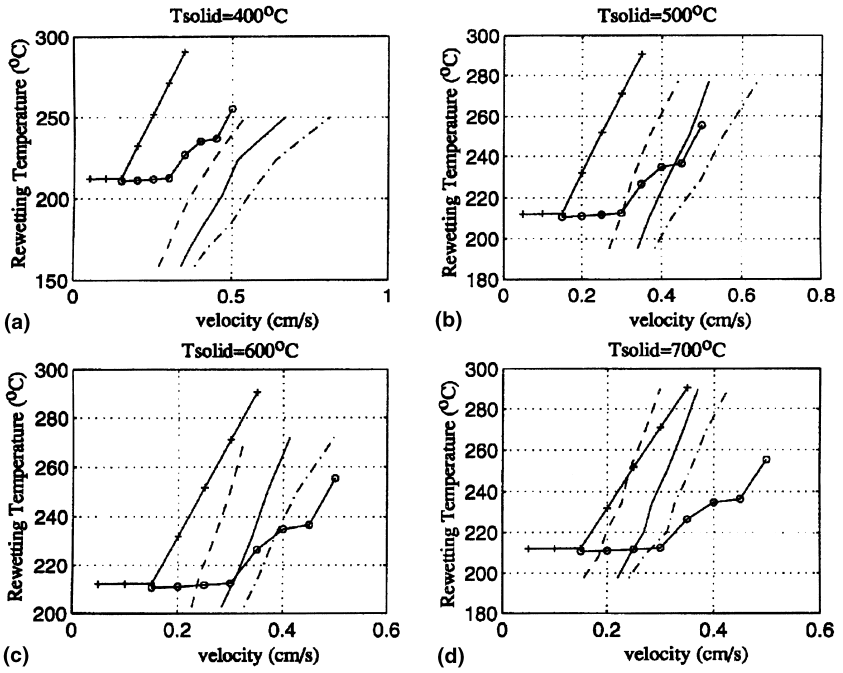

Fig. 22. Determination of quench velocity and rewetting temperature by intersection of quench velocity–temperature relations: water on stainless steel at different values of flow rate and initial solid temperatures (a)–(d). Macro model (flow rate, per unit wetted perimeter (kg/ms)): – – 0.017; – 0.047; —– 0.11. Micro model (solid–liquid interaction parameter, ε_ω/kT_c): ∘∘ 4.1; ++ 4.9.

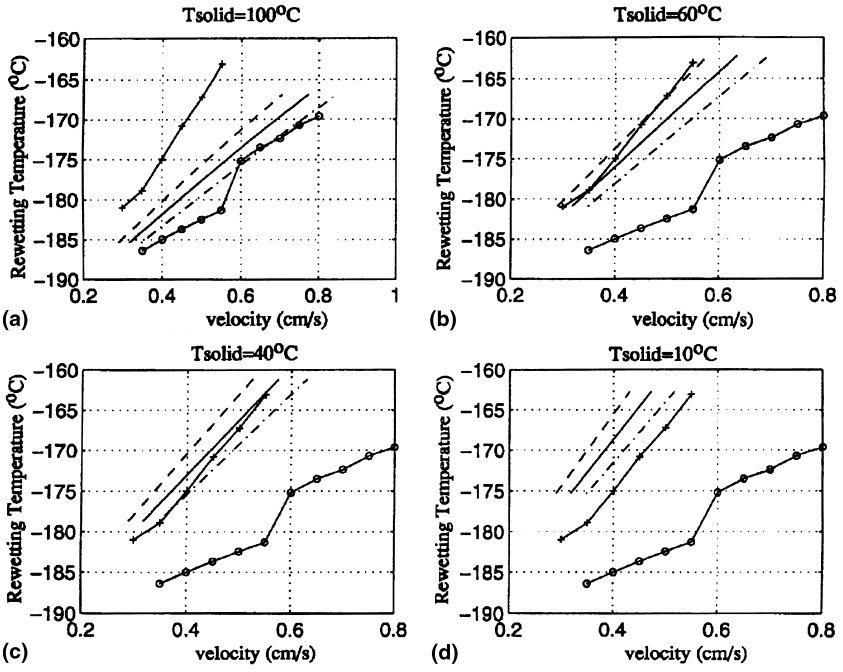

Fig. 23. Determination of quench velocity and rewetting temperature by intersection of quench velocity–temperature relations: nitrogen on copper at different values of flow rate and initial solid temperature (a)–(d). Macro model (flow rate per unit wetted perimeter, (kg/ms)): – – 0.12; – 0.20; —– 0.36. Micro model (solid–liquid interaction parameter, ε_ω/kT_c): ∘∘ 4.1; ++ 4.9.

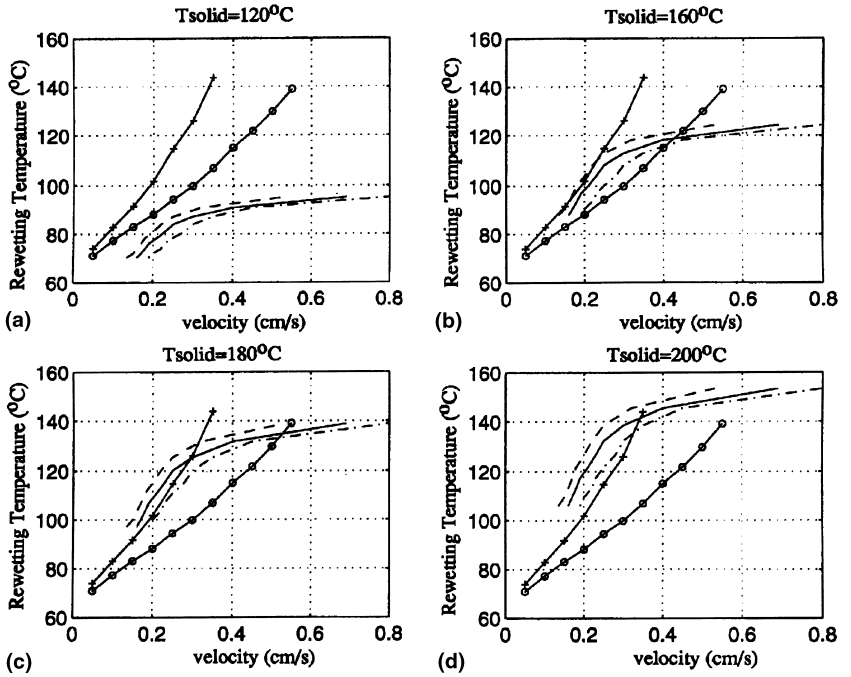

Fig. 24. Determination of quench velocity and rewetting temperature by intersection of quench velocity–temperature relations: for Freon-113 on stainless steel at different values of flow rate and initial solid temperature (a)–(d). Macro model (flow rate per unit wetted perimeter, (kg/ms)) – – 0.13; – 0.25; –– 0.45. Micro model (solid–liquid interaction parameter, ε_ω/kT_c): ○○ 4.1; ++ 4.9.

mines uniquely the quench velocity and rewetting temperature, U^*_{rew} and T^*_{rew}, for each specific solid–liquid system that is investigated. The location of this point is a function of several parameters. Typical effects of these parameters on U^*_{rew} and T^*_{rew} are illustrated and discussed in the following.

3.5.1. Effect of the initial solid temperature

The two micro-model curves (in Figs. 22–24) depend on one micro parameter, ε_ω/kT_c, that stands for the magnitude of the intermolecular solid–liquid interaction. Higher values of the initial solid temperature, T_{solid}, irrespective of the flow rate, produce lower values of U^*_{rew} and T^*_{rew}. Consequently, the location of the intersection point shifts to the left. This is due to the higher heat fluxes, at the triple phase contact region, which cause higher evaporation rates. The quenching process becomes slower, and hence, U^*_{rew} is expected to decrease. For example, in the case of nitrogen on copper, see Fig. 23(b), at $\varepsilon_\omega/kT_c = 4.9$ and $T_{solid} = -60°C$, the values of U^*_{rew} and T^*_{rew} are: 0.35, 0.5 cm/s and approximately −178°C, −167°C, for the flow rates of 0.20 and 0.12 kg/ms, respectively. In Fig. 23(c), the initial solid temperature is $T_{solid} = -40°C$, and the values of U^*_{rew} and T^*_{rew} are approximately 0.38, 0.55 cm/s and −176°C, −162°C, for the two flow rates of 0.36 and 0.20 kg/ms, respectively. A similar behavior is observed for water on stainless steel (see Fig. 22). In Fig. 22(b), $T_{solid} = 500°C$ and $\varepsilon_\omega/kT_c = 4.1$, and the values obtained for U^*_{rew} and T^*_{rew}, for the flow rate 0.047 kg/ms are 0.42 cm/s and 235°C. Increasing the solid temperature to $T_{solid} = 600°C$ (illustration (c)), shows that U^*_{rew} and T^*_{rew} are shifted leftward, to 0.32 cm/s and 215°C.

3.5.2. Effect of the flow rate

Higher values of the quench velocity and rewetting temperature are expected at higher flow rates. For example, in Fig. 23(c), the two values of the flow rate of nitrogen on copper 0.12, 0.2 kg/ms, produce the following two values for U^*_{rew} and T^*_{rew}: 0.38, 0.55 cm/s, and approximately −177°C, −162°C. The higher values of T_{rew} are associated with smaller heat fluxes in the triple phase contact region. This implies that the evaporation is bound to be less intense, due to the decreased heat fluxes, and consequently, the value of U^*_{rew} is expected to be higher. Thus the rise in T^*_{rew} is associated with a corresponding increase in U^*_{rew}.

3.5.3. Effect of intermolecular attraction

The third parameter which determines the quench velocity and the rewetting temperature is the solid–liquid intermolecular attraction, represented by ε_ω/kT_c. Figs. 22–24 show that larger values of this parameter, lead to a shift of the intersection point between the macro and micro models to the right. In other words, at fixed initial solid temperature and flow rate, larger values of ε_ω/kT_c

produce higher values of U^*_{rew} and T^*_{rew}. For example, consider the case of water on stainless steel, Fig. 22(d), $T_{solid} = 700°C$. At a flow rate of 0.017 kg/ms and $\varepsilon_\omega/kT_c = 4.1$, the values of T^*_{rew} and U^*_{rew} are ~210°C and 0.2 cm/s. At $\varepsilon_\omega/kT_c = 4.9$ these values increase to 250°C and 0.25 cm/s. Larger values of ε_ω/kT_c indicate rewetting situations where the solid–liquid intermolecular attraction forces are stronger. This means that given the same macro-scale operating conditions (T_{solid}, flow rate, etc.), the contact between the solid and liquid molecules can exist at higher temperatures, and hence, T^*_{rew} is also higher. The increased value of T^*_{rew} entails reduced heat fluxes, this being due to the lower temperature gradients that exist at the triple contact phase region. Consequently, the evaporation is weaker and the expected value of U^*_{rew} increases. The possibility of multiple solutions for U^*_{rew}, T^*_{rew} is implied in Fig. 24, where the macro and micro models can intersect at more than one point.

In this context, the comparison between different ε_ω/kT_c curves must be done, using the first physically possible intersection points. For example, in Fig. 24(b)–(d), these intersection points can be obtained by extending the macro-scale curves toward the region of lower velocity. As explained below, the higher values are not physical. At 0.25 kg/ms (see Fig. 24(c)), this extension gives $U^*_{rew} = 0.15$ cm/s, $T^*_{rew} = 90°C$, and $U^*_{rew} = 0.10$ cm/s, and $T^*_{rew} = 80°C$ at $\varepsilon_\omega/kT_c = 4.9$ and 4.1, respectively.

3.5.4. Conditions for existence of rewetting

The parameter ε_ω/kT_c also determines, given the operating conditions, the existence or exclusion of rewetting. For example, consider the case of Freon-113 on stainless steel at $T_{solid} = 120°C$ shown in Fig. 24(a). Here, the macro and micro curves do not intersect and hence, no rewetting can exist. This result can be interpreted in the following way: the values taken for ε_ω/kT_c constrain the system to have attraction forces between the solid and liquid molecules, which are strong enough to raise the microscopically feasible rewetting temperature above the one predicted by the macro model. In this case, the weaker temperature gradients and lower heat fluxes, dictated by the operating conditions, are insufficient to evaporate the liquid fast enough, and the system turns into one of "complete" wetting. When the initial solid temperature, T_{solid}, is increased from 120°C to 160°C (see Fig. 24(b)), the micro curves (fixed ε_ω/kT_c) remain unchanged while the macro curves rise and intersect them. This means that at $T_{solid} = 160°C$ rewetting can exist in the Freon-113/stainless steel system. Here, the increase in temperature gradient enhances the heat flux, and hence also the rate of evaporation, to the level that facilitates the existence of a rewetting situation.

Fig. 24(b) shows one and two intersection points for the same set of macro–micro curves. The occurrence of multiple solutions can be linked to stability considerations. Here the system may switch between the solutions, e.g., from the less stable to the more stable state. However, further investigation of this phenomenon is outside the scope of this work. High enough levels of T_{solid} that raise the macro curves above the micro curves prevent, once again, intersection. In this case, rewetting cannot exist and conditions of non-wetting prevail. Another explanation is based on the intermolecular forces: lower values of ε_ω/kT_c indicate weaker solid–liquid attraction forces, and hence, the predicted values of T_{rew} by the micro curves, are also lower. Consequently, given the value of T_{solid}, higher temperature gradients are expected at the triple phase contact region, which lead to higher heat and evaporation fluxes. In this case, the intensive evaporation is sufficient to prevent rewetting through the solid–liquid contact. Increase of ε_ω/kT_c, at high levels of T_{solid}, lifts the micro curves so that their intersection with the macro curves becomes feasible again.

4. Summary and conclusions

4.1. Combined hydrodynamic–theromodynamic micro-scale algorithm

The new algorithm of a combined model which links the micro-scale hydrodynamic and thermodynamic models is used to establish an important relation between a postulated, or rather imposed, quench velocity and its corresponding rewetting temperature. Calculations were performed by using the new combined model for several categories of liquids with diverse thermo-physical properties (alcohols, polar, hydrocarbons, liquefied gases and fluorocarbons), and the predicted rewetting temperatures, corresponding to the postulated quench velocities, show a satisfactory agreement with experimental data and other models. For each postulated value of quench velocity, a single value of rewetting temperature is predicted. The monotonous, nearly linear, quench velocity–rewetting temperature relation, which is characterized by a positive slope, reflects the physics of the rewetting system. The decrease in contact angle, due to a rise in temperature, is in agreement with experimental observations, which were compiled from several sources. Higher values of the intermolecular forces parameter ε_ω/kT_c, induce higher rewetting temperatures and smaller values of contact angle, corresponding to flatter films. The case of helium is unique because of its special thermo-physical properties. Both the liquid–vapor interfacial tension (0.12×10^{-3} N/m) and the maximum superheat (~1°C) are exceptionally small as compared to other liquids. The new model provides results that compare very well with experimental data. In view of the small temperature

increments used in the iterations for helium, $\Delta T^* = 0.001°C$, the sensitivity of the results is a remarkable outcome of the new model. In this sense, the helium case is an excellent example showing the validity of the model performance.

The MS of the liquid film shows a unique behavior, in a rather narrow range. For example, MS values corresponding to the tested fluorocarbons and alcohols, were $\sim$0.006 and $\sim$0.003, respectively. In summary, the combined micro-scale thermodynamic–hydrodynamic algorithm presented here consists of a new approach for prediction of the rewetting temperature. In this algorithm, heat transfer, physico-chemical phenomena and micro-hydrodynamic considerations were integrated into a unified model. This approach is combined with a macro-scale rewetting model, in order to determine U_{rew} and T_{rew}, simultaneously.

4.2. Integrated approach for rewetting systems

The main goal of the work reported here, and in previous parts of this series [1,2] is the investigation, characterization and simulation of the phenomena occurring at the quench front during rewetting of hot surfaces. The new thermodynamic–hydrodynamic micro-scale model is interfaced with a macro-scale model for the simultaneous determination of the rewetting temperature and quench velocity. In contrast to the classical approaches, which treat the rewetting process as either a hydrodynamic or a thermodynamic problem, the efforts here were focused on finding an integrated approach, through the combined use of principles of thermodynamics, hydrodynamics, interfacial phenomena and heat transfer.

The hydrodynamic model is combined with the micro-scale thermodynamic model of Sullivan that is based on statistical–mechanical principles [9,10]. The combined model yields a relation between solution of the rewetting temperature that corresponds to a postulated quench velocity. This derived relation is an important consequence of the new combined approach. In most of the available rewetting models, both the rewetting temperature, T_{rew}, and the heat transfer coefficient are needed as input for the calculation of the quench front velocity, U_{rew}. The model of Olek et al. [4] is more advanced, in the sense that only T_{rew} is required as input, while the heat transfer coefficient is obtained as part of the solution. In our new model, both variables are not required as input data and a relation between T_{rew} and U_{rew} is obtained from basic principles. The interfacing of the micro-scale model, with a known macro-scale model, facilitates the simultaneous determination of T^*_{rew} and U^*_{rew}, for a wide range of solid–liquid systems and operating conditions. This was verified here for several diverse solid–liquid systems, which were tested using the new micro-scale model that was interfaced with the macro-scale model of Olek et al. [4]. In this context, a new criterion for existence of rewetting was defined.

The values of T^*_{rew} and U^*_{rew} were determined at the points of intersection between the micro- and macro-scale curves relating to these variables. Such intersection is postulated to set the condition for existence of rewetting. If no such intersection is possible, then either complete wetting or complete non-wetting prevails so that no rewetting can occur.

The performance of the micro model was tested with diverse groups of solid–liquid systems. For example, in this series, organic, inorganic, polar and cryogenic liquids were investigated. The results predicted by the new model, which include rewetting temperatures, quench front velocities, contact angles, etc., show a satisfactory agreement with experimental data and with other theoretical models.

The micro-scale thermodynamic–hydrodynamic treatment presented here, shows that the rewetting temperature of hot surfaces cannot be determined using data that is limited to fluid properties and flow conditions (as assumed by the separate hydrodynamic or thermodynamic approaches). It strongly depends on the solid–liquid interaction, through the intermolecular forces (long range forces and repulsive ones) which are usually ignored in macroscopic models. These forces contribute significantly to the physical mechanisms that govern the rewetting process. Stronger intermolecular forces (larger Hamaker constant) entail higher rewetting temperatures. The stronger attraction forces enable the liquid molecules to stay in contact with hotter solid surfaces, and consequently the rewetting temperature is higher.

This work establishes the link between the conditions that allow micro-scale rewetting and those that are imposed by macro-scale operating conditions. The interfacing between the two models is the essence of this new approach for the solution of rewetting problems. A basic feature of the new approach is that it relies completely on the thermo-physical properties of the solid–liquid–vapor rewetting system, and on its operating conditions. The new approach is free of the need for assumptions regarding the value of either T_{rew} or U_{rew}, as both are obtained uniquely as its output.

Appendix A. Calculation procedure of the bulk temperature, T_b

The thermodynamic contact angle, θ_t, is determined by Sullivan's model using the temperature of the solid–liquid system. This temperature is expressed non-dimensionally by T_b/T_c. The bulk temperature, T_b, is defined as an average temperature over the region

considered ($0 \leqslant \xi \leqslant 1,\ 0 \leqslant z \leqslant h(\xi)$, dimensionless). The dimensionless bulk temperature, Θ_b, is defined by the following expression:

$$\Theta_b = \frac{\int_0^1 \int_0^{h(\xi)} \Theta(\xi, z)\, d\xi\, dz}{\int_0^1 \int_0^{h(\xi)} d\xi\, dz}, \tag{A.1}$$

where $h(\xi)$ is the interface profile, given in a system of coordinates that is attached to the contact line and determined by the solution of the micro-scale hydrodynamic model [2]. Inserting Eq. (9) for $\Theta(\xi, z)$ into Eq. (A.1), Θ_b is determined explicitly as

$$\begin{aligned}\Theta_b &= \frac{\int_0^1 \int_0^{h(\xi)} (1 + N(h - z))/(1 + Nh)\, d\xi\, dz}{\int_0^1 h(\xi)\, d\xi} \\ &= 1 - \frac{[\int_0^1 (Nh^2/2(1 + Nh))\, d\xi]}{\left[\int_0^1 h(\xi)\right] d\xi}.\end{aligned} \tag{A.2}$$

The integrals in Eq. (A.2) can be calculated numerically in terms of the profile solution, $h(\xi)$, of the interface.

Appendix B

Consider a rod, or a flat plate, that is subjected to top flooding (Fig. 21). The essential features of their macroscale theory are outlined briefly as follows [4].

The following formulation is valid both for Cartesian and cylindrical coordinate systems. The two-dimensional energy equations for the solid and the liquid, respectively, are

$$\begin{aligned}&\frac{\partial \overline{T}_1}{\partial \overline{t}} = \overline{\alpha}_1 \left[\frac{1}{\overline{r}^v} \frac{\partial}{\partial \overline{r}} \left(\overline{r}^v \frac{\partial \overline{T}_1}{\partial \overline{r}}\right) + \frac{\partial^2 \overline{T}_1}{\partial \overline{x}^2}\right], \\ &0 \leqslant \overline{r} \leqslant \overline{r}_1,\ -\infty < \overline{x} < \infty,\ \overline{t} > 0\end{aligned} \tag{B.1}$$

and

$$\begin{aligned}&\frac{\partial \overline{T}_2}{\partial \overline{t}} + \overline{v} \frac{\partial \overline{T}_2}{\partial \overline{x}} = \overline{\alpha}_2 \left[\frac{1}{\overline{r}^v} \frac{\partial}{\partial \overline{r}} \left(\overline{r}^v \frac{\partial \overline{T}_2}{\partial \overline{r}}\right) + \frac{\partial^2 \overline{T}_2}{\partial \overline{x}^2}\right], \\ &\overline{r}_1 \leqslant \overline{r} \leqslant \overline{r}_2,\ -\infty < \overline{x} \leqslant 0,\ \overline{t} > 0,\end{aligned} \tag{B.2}$$

where the overbar indicates a dimensional variable and

$$v = \begin{cases} 0 & \text{for a Cartesian geometry,} \\ & \quad \text{with } \overline{r} \equiv \overline{z}, \overline{r}_1 \equiv \overline{\delta}_1, \overline{r}_2 \equiv \overline{\delta}_2, \\ 1 & \text{for a cylindrical geometry.} \end{cases}$$

The subscripts 1 and 2 denote the solid and the liquid, respectively, A denotes the region above (behind) the quench front, both in the solid and in the liquid, and B denotes the "dry region" in the solid, below (ahead of) the quench front. The thermal diffusivity is denoted by $\overline{\alpha}$, $\overline{T}$ denotes temperature, $\overline{t}$ is the time, $\overline{x}$ and $\overline{r}$ the space coordinates, U_{rew} the fixed quench front velocity (a quasi-steady state assumption), and $\overline{v}$ denotes the average velocity of the liquid film. All these variables are dimensional. Applying the quasi-steady-state assumption ($\partial \overline{T}/\partial \overline{t} = -U_{rew} \partial \overline{T}/\partial \overline{x}$), Eqs. (B.1) and (B.2) take the following form:

$$\begin{aligned}&\frac{1}{\overline{r}^v} \frac{\partial}{\partial \overline{r}} \left(\overline{r}^v \frac{\partial \overline{T}}{\partial \overline{r}}\right) + \frac{\partial^2 \overline{T}}{\partial \overline{x}^2} + \frac{\overline{u}_i}{\overline{\alpha}_i} \frac{\partial \overline{T}}{\partial \overline{x}} = 0, \\ &0 \leqslant \overline{r} \leqslant \overline{r}_2,\ -\infty < \overline{x} < \infty,\end{aligned} \tag{B.3}$$

$$\overline{u}_i = \begin{cases} U_{rew}, \\ U_{rew} - \overline{v}, \end{cases} \quad \overline{\alpha}_i = \begin{cases} \overline{\alpha}_1, & 0 \leqslant \overline{r} \leqslant \overline{r}_1, \\ \overline{\alpha}_2, & \overline{r}_1 \leqslant \overline{r} \leqslant \overline{r}_2. \end{cases} \tag{B.4}$$

Olek et al. [4] defined the following normalized variables:

$$\Theta \equiv \frac{\overline{T} - \overline{T}_{in}}{\overline{T}_w - \overline{T}_{in}}, \quad r \equiv \frac{\overline{r}}{\overline{r}_2}, \quad r_1 \equiv \frac{\overline{r}_1}{\overline{r}_2}, \quad x \equiv \frac{\overline{x}}{\overline{r}_2}, \tag{B.5}$$

where $\overline{T}_w$ is the initial solid temperature (far ahead of the quench front), and $\overline{T}_{in}$ is the liquid inlet temperature. By virtue of Eq. (B.5), the energy Eq. (B.3) is transformed into the following dimensionless form:

$$\frac{1}{r^v} \frac{\partial}{\partial r} \left(r^v \frac{\partial \Theta}{\partial r}\right) + \frac{\partial^2 \Theta}{\partial x^2} + u(r) \frac{\partial \Theta}{\partial x} = 0, \tag{B.6}$$

where

$$u(r) = \begin{cases} u_1 = U_{rew} \overline{r}_2 / \overline{\alpha}_1, & 0 \leqslant r \leqslant r_1, \\ u_2 = (U_{rew} - \overline{v}) \overline{r}_2 / \overline{\alpha}_2, & r_1 \leqslant r \leqslant 1. \end{cases} \tag{B.7}$$

Note that all variables without overbar are dimensionless.

Eq. (B.6) is solved with the following boundary conditions:

$$r = 0,\ -\infty < x \leqslant 0: \quad \frac{\partial \Theta_A}{\partial r} = 0, \tag{B.8}$$

$$r = 1,\ -\infty < x \leqslant 0: \quad \Theta_A = 0, \tag{B.9}$$

$$r = r_1,\ -\infty < x \leqslant 0: \quad \Theta_A^- = \Theta_A^+, \tag{B.10a}$$

$$r = r_1,\ -\infty < x \leqslant 0: \quad \frac{\overline{\lambda}_1}{\overline{\lambda}_2} \frac{\partial \Theta_A^-}{\partial r} = \frac{\partial \Theta_A^+}{\partial r}, \tag{B.10b}$$

$$x \to -\infty,\ 0 \leqslant r \leqslant 1: \quad \Theta_A \to 0, \tag{B.11}$$

$$x = 0,\ 0 \leqslant r \leqslant r_1: \quad \Theta_A = \Theta_B, \tag{B.12a}$$

$$x = 0,\ 0 \leqslant r \leqslant r_1: \quad \frac{\partial \Theta_A}{\partial x} = \frac{\partial \Theta_B}{\partial x}, \tag{B.12b}$$

$$x = 0,\ r_1 < r \leqslant 1: \quad \Theta_A = f(r) = \frac{F(\bar{r}) - \overline{T}_{in}}{\overline{T}_w - \overline{T}_{in}}, \qquad (B.13)$$

$$r = 0,\ 0 \leqslant x < \infty: \quad \frac{\partial \Theta_B}{\partial r} = 0, \qquad (B.14)$$

$$r = r_1,\ 0 \leqslant x < \infty: \quad \frac{\partial \Theta_B}{\partial r} = 0, \qquad (B.15)$$

$$x \to \infty,\ 0 \leqslant r \leqslant r_1: \quad \Theta_B = 1, \qquad (B.16)$$

$$x = 0,\ r = r_1: \quad \Theta_B = \Theta_0 \text{ or } \Theta_A = \Theta_0, \qquad (B.17)$$

where $\overline{\lambda}_1$ and $\overline{\lambda}_2$ are the thermal conductivities of the solid and the liquid, respectively, the superscripts + and − denote the left- and right-hand sides along the solid–liquid interface ($r = r_1$), and Θ_0 is the dimensionless rewetting (quench) temperature, corresponding to T_{rew}. It is emphasized that in this model, as in all previous rewetting models, it was necessary to assume that T_{rew} is known (given value). The above system of equations was solved analytically by Olek et al. [4] using series expansion. Several functions for $f(r)$, Eq. (B.13), have been used and the effect of changing them on the results was found to be negligible. The profile $f(r)$ which was used here is linear, between the values Θ_0 and Θ_s (saturation temperature), in the range $r_1 < r \leqslant 1$.

The solution procedure was as follows: first, Eqs. (B.1)–(B.16) are solved, by the special series expansion as an eigenvalue problem, to yield the temperature field (in the three regions) in terms of the unknown rewetting velocity, U_{rew}. Then, condition Eq. (B.17) is applied to obtain U_{rew} as a function of T_{rew}, taken as an arbitrary input parameter. In this way, using realistic operating conditions, and empirical data for the rewetting temperature, Olek et al. [4] found rewetting velocities for various solid–liquid pairs.

In the present work, the above macro-scale model of Olek et al. [4] was used to derive one relation for $U_{rew}(T_{rew})$. This is coupled with a relation, derived from our micro-scale model [1,2] to determine uniquely the values of U^*_{rew} and T^*_{rew}.

References

[1] M. Ben David, Y. Zvirin, Y. Zimmels, Determination of the quench velocity and rewetting temperature of hot surfaces: formulation of non-isothermal microscale hydrodynamic model, Phys. Rev. E. 59 (1999) 6687–6698.

[2] M. Ben David, Y. Zimmels, Y. Zvirin, Determination of the quench velocity and rewetting temperature of hot surfaces. Part I: analytical solution of the micro-scale hydrodynamic model, Int. J. Heat Mass Transfer 44 (2001) 1323–1342.

[3] J.J. Carbajo, A study of the rewetting temperature, Nucl. Eng. Design 84 (1985) 21–52.

[4] S. Olek, Y. Zvirin, E. Elias, Rewetting of hot surfaces by falling liquids films as a conjugate heat transfer problem, Int. J. Multiphase Flow 14 (1988) 13–33.

[5] V. Gerweck, Rewetting phenomena and their relation to intermolecular forces between a hot wall and the fluid, Paul Scherrer Institute, Wurenlingen and Villigen Bericht Nr. 42, 1989.

[6] G. Yadigaroglu, M. Adrenai, S.N. Akson, M.J. Lewis, G.Th. Analytis, D. Lubbesmeyer, S. Olek, Modeling of thermohydraulic emergency core cooling phenomena, PSI – Paul Scherrer Institut-Berict Nr. 27, 1990.

[7] V. Gerweck, G. Yadigaroglu, A local equation of state for a fluid in the presence of a wall and its application to rewetting, Int. J. Heat Mass Transfer 35 (1992) 1823–1832.

[8] M. Ben David, Investigation of the phenomena at the quench front of hot surfaces. D.Sc. Thesis, Technion – Israel Institute of Technology, Haifa, Israel, 1997.

[9] D.E. Sullivan, van der Waals model of adsorption, Phys. Rev. B 20 (1979) 3991–4000.

[10] D.E. Sullivan, Surface tension and contact angle of a liquid solid interface, J. Chem. Phys. 74 (1981) 2604–2615.

[11] R.C. Weast, M.J. Astle, CRC Handbook of Chemistry and Physics, 62nd ed., CRC Press, Boca Raton, FL, 1981–1982.

[12] B.C. Harold, Handbook of Thermodynamic Tables and Charts, Hemisphere, Washington, DC, 1976.

[13] J.O. Hirschfelder, C.F. Curtiss, B.R. Byron, Molecular Theory of Gases and Liquids, fourth ed., Wiley, New York, 1967.

[14] S. Olek, Y. Zvirin, E. Elias, The relation between rewetting temperature and the liquid–solid contact angle, Int. J. Heat Mass Transfer 31 (1988) 898–902.

[15] R.B. Duffey, D.T.C. Porthouse, The physics of rewetting in water reactor emergency core cooling, Nucl. Eng. Design 25 (1972) 379–394.

[16] S. Yao, R.E. Henry, An investigation of the minimum film boiling temperature on horizontal surfaces, J. Heat Transfer 100 (1978) 260–267.

[17] K.J. Baumeister, F.F. Simon, Leidenfrost temperature – its correlation for liquid metals, cryogenics hydrocarbon and water, J. Heat Transfer 94 (1973) 166–173.

[18] B.J. Stock, Observations on transition boiling heat transfer phenomena, ANL-6175, Argonne National Laboratory, Argonne, IL, 1960.

[19] S.E. Simopoulos, A.A. El-Sherbini, W. Murgatroyd, Experimental investigation of the rewetting process in a Freon-113 vapour environment, Nucl. Eng. Design 55 (1979) 17–24.

[20] L. Manson, Correlation of shrouded spherical vessels in liquid nitrogen, Advances in Cryogenic Engineering, vol. 12, Plenum Press, New York, 1967, pp. 373–380.

[21] R.E. Henry, A generalized correlation for the minimum film boiling temperature, in: ASME, AIChE 1973, 14th National Heat Transfer Conference, Atlanta, GA.

[22] D.S. Dunga, R.H.S. Winterton, Measurement of surface contact in transition boiling, Int. J. Heat Mass Transfer 28 (1985) 1869–1880.

[23] G.J. Capone, E.L. Park Jr., Film boiling of Freon 113, normal pentane cyclopentane and benzene from cylindrical surfaces at moderate pressures, Int. J. Heat Mass Transfer 22 (1979) 121–129.

[24] H. Carslaw, J. Jaeger, Conduction of Heat in Solids, second ed., Clarendon Press, Oxford, 1959.
[25] M.E. Swan, M.W. Carbon, A review of spray-cooling and bottom flooding work for LWR cores, Nucl. Eng. Design 32 (1975) 191–207.
[26] D. Butterworth, R.G. Owen, The quenching of hot surfaces by top and bottom flooding – a review, Report No. AERE – R7992, AERE Harwell, Oxon, 1975.
[27] E. Elias, G. Yadigaroglu, A general one-dimensional model for conduction-controlled rewetting of surface, Nucl. Eng. Design 42 (1977) 185–194.
[28] E. Elias, G. Yadigaroglu, The reflooding phase of LOCA in PWRs Part II. Rewetting and liquid entrainment, Nucl. Safety 19 (1978) 160–175.
[29] J.J. Carbajo, A.D. Siegel, Review and comparison among the different models for rewetting in LWRs, Nucl. Eng. Design 58 (1980) 33–44.
[30] S. Olek, Rewetting of hot surfaces, D.Sc. Thesis, Technion – Israel Institute of Technology, Haifa, Israel, 1986.